Analysis of Loss Processes in GaN-based LEDs

Von der Fakultät für Elektrotechnik, Informationstechnik, Physik
der Technischen Universität Carolo-Wilhelmina zu Braunschweig

zur Erlangung des Grades eines Doktors
der Naturwissenschaften (Dr. rer. nat.)

genehmigte Dissertation

von Ailun Zhao

aus Hebei,China

eingereicht am: 17.08.2016

Disputation am: 24.11.2016

1. Referent: Prof. Dr. A. Hangleiter
2. Referent: Prof. Dr. S. Kück

Druckjahr 2016

Dissertation an der Technischen Universität Braunschweig,
Fakultät für Elektrotechnik, Informationstechnik, Physik

Tagungsbeiträge:

- A. Zhao, U. Rossow, and A. Hangleiter?Investigation of efficiency of blue and green LEDs (Poster), DPG spring meeting, Berlin (2012)
- A. Zhao, U. Rossow, H. Bremers, and A. Hangleiter, Investigation of extraction efficiency and internal quantum efficiency of GaN-based LEDs (Presentation), DPG spring meeting, Regensburg(2013)
- A. Zhao, U. Rossow, H. Bremers, and A. Hangleiter, Investigation of recombination processes in QW of GaN-based LEDs (Poster), IGSM summer school (2014)

Contents

Zusammenfassung

GaN-basierte Leuchtdioden (LEDs) haben sehr große Aufmerksamkeit hervorgerufen und sind in den letzten Jahren sehr schnell weiterentwickelt worden, weil sie in Hinblick auf Energieeinsparung und Stabilität vorteilhaft sind. Es bleiben jedoch noch einige Herausforderungen wie z.B. das sogenannte "green gap" und der Einbruch der Effizienz bei hohen Stromdichten ("efficiency droop"), die Anwendungen von diesen LEDs bei größeren Wellenlängen bzw. hoher Leistung noch einschränken. Um diese Probleme zu lösen, ist ein grundlegendes Verständnis der Rekombinationsprozesse von Elektronen und Löchern in der aktiven Region erforderlich. Zu diesem Zweck ist eine zuverlässige Bestimmung der internen Quanteneffizienz, der Ladungsträgerdichte innerhalb Quantentröge in LEDs und der Lebensdauer der strahlenden und nicht-strahlenden Rekombination sehr hilfreich, um Rekombinationsprozesse besser zu verstehen. Der Hauptteil dieser Arbeit beschäftigt sich mit folgenden Aspekten:

Zuerst wird eine zuverlässige Auskoppeleffizienz für unsere LED-Struktur mit einem einzelnen Quantentrog über die Berechnung und Kalibrierung erhalten. Gemäß der Theorie der Lichtausbreitung in verschiedenen Medien wird die Auskoppeleffizienz mit der bekannten Struktur unserer LED berechnet. Für die Berechnung sind die komplexen dielektrischen Funktionen von GaN, Saphir und Pt, die Dispersion der dielektrischen Funktionen und die TE Polarisation der Emission berücksichtigt worden. Die Ergebnisse zeigen, dass wegen des hohen Brechungsindex von GaN und der internen Totalreflexion ein sehr kleiner Austrittswinkel des Lichts resultiert und damit die Auskoppeleffizienz ziemlich niedrig ist. Bei der Berechnung wird davon ausgegangen, dass jede Grenzfläche im Schichtenstapel der LED ideal scharf und glatt und die Reflexion der Metallschicht endlich ist. Eine Kalibrierung ist notwendig, da die reale von der idealen Struktur abweichen könnte und damit z.B. die Phasenverschiebung bei der Reflexion von Licht an der Metallschicht oder ein reduziertes Reflexionsvermögen aufgrund von Rauigkeit der Grenzfläche zwischen GaN und Metall auftreten könnte. Eine Probenserie wurde gewachsen mit nominell gleicher Struktur, aber unterschiedlicher GaN Kontaktschichtdicke. Bei gleicher interner Quanteneffizienz variiert damit die Auskoppeleffizienz. Durch eine Skalierung der berechneten Auskoppel-

effizienz mit den Werten aus dem Experiment wird eine zuverlässige Auskoppeleffizienz erhalten.

Zweitens entwickelten wir eine Prozedur um die Ladungsträgerdichte bei verschiedenen Injektionsströmen zu bestimmen. Rekombinationsprozesse von Elektronen und Löchern in Quantentrögen in LEDs hängen stark von der Ladungsträgerdichte in der aktiven Zone ab. Es ist für ein besseres Verständnis der Rekombination nötig, einen zuverlässigen Wert für die Ladungsträgerdichte in dem Quantentrog zu haben. Effekte des elektrischen Feldes im p-n-Übergang, das piezoelektrische Feld und die von den freien Ladungsträgern verursachte Abschirmung der elektrischen Felder auf die Lage der Emissionsenergie sind untersucht worden. Es ist gut bekannt, dass ein piezoelektrisches Feld eine Rotverschiebung der Emissionsenergie verursacht. Das elektrische Feld des p-n Überganges hat ein dem piezoelektrische Feld entgegengesetztes Vorzeichen. Sie haben also einen abschirmenden Effekt. Die Stärke der Abschirmung hängt von der Ladungsträgerdichte ab. Die Abhängigkeit der Emissionsenergie von der Ladungsträgerdichte wird berechnet, wobei das Feld des p-n Überganges, das piezoelektrische Feld und der abschirmende Effekt der Ladungsträger berücksichtig wird. Nach der Berechnung gibt es ein Minimum der Emissionsenergie als Funktion der Ladungsträgerdichte. Dies ist so weil das p-n Übergangsfeld abnimmt und die Abschirmung linear zunimmt durch die freie Ladungsträgerdichte und dann dominant wird. Eine minimale Emissionsenergie in der elektrisch betriebenen Struktur ist tatsächlich beobachtet worden wenn der Strom von sehr kleinen Werten zu sehr großen Werten geändert wurde. Aus einem Vergleich der Simulation und Messung des Minimums konnten korrekte Werte für die Ladungsträgerdichte gefunden werden. Damit konnte dann für eine Probe die Ladungsträgerdichte erfolgreich bestimmt werden.

Drittens konnte die Abhängigkeit der strahlenden und nicht-strahlenden Lebensdauer von der Ladungsträgerdichte untersucht werden mit der oben genannten Vorgehensweise. Die Stromdichten der strahlenden und nicht-strahlenden Prozesse konnten aus der Gesamtstromdichte mit Hilfe der internen Quanteneffizienz extrahiert werden. Für jede bei einer bestimmten Vorwärtsstromdichte gemessene Emissionsenergie konnte die Ladungsträgerdichte errechnet werden und daraus die strahlenden und nicht-strahlenden Lebensdauern. Bei der strahlenden Rekombination zeigt die Abhängigkeit der Lebensdauer von der Ladungsträgerdichte, dass das elektrische Feld den Überlapp der Elektronen- und Loch-Wellenfunktionen im Quantentrog beeinflusst.

Die nicht-strahlende Rekombination ist unklar. Ein merkwürdiges Verhalten der Abhängigkeit der nicht-strahlenden Lebensdauer von der Ladungsträgerdichte wurde beobachtet: die

nicht-strahlende Lebensdauer ist nicht konstant bei kleinen Ladungsträgerdichten für einige Proben, was nicht erklärt werden kann. Weitere Untersuchungen und Überprüfungen sind nötig bei diesen Proben.

Abstract

GaN-based light-emitting diodes (LEDs) have attracted huge attention and developed rapidly in recent years due to advantages as light source regarding energy-saving and stability. However, several challenges still remain such as the "green gap" and "efficiency droop", which have seriously restrict further applications of LEDs towards longer wavelength and high power. In order to overcome these problems, a fundamental understanding of recombination processes of electrons and holes in the active region is required. Therefore, a reliable determination of the internal quantum efficiency, carrier density within the quantum wells in the LED structure, and radiative and nonradiative recombination lifetimes are quite helpful to further understand recombination processes. The main part of this thesis focusses on the following aspects:

First a reliable value for the extraction efficiency for our single quantum well LED structure is obtained via calculation and calibration. According to the theory of light propagation in different media, the extraction efficiency is calculated based on the LED structure. For the calculation the complex dielectric functions of GaN, sapphire, and Pt, the dispersion of the dielectric functions and TE polarization of the emission are taken into account. The results of the calculation show that the extraction efficiency is rather low since the high refractive index of GaN and the total internal reflection lead to a very small escape angle for the emitted light. In the calculations the interfaces of the different layers in LED structure are assumed to be ideal sharp and flat and the reflection of metallic contact layer is finite. A calibration is necessary because the real structure may be different from the ideal one. This may affect the e.g. phase shift in the reflection of light at the metallic layer and an reduced reflectivity due to roughness of the interface between GaN and the metal contact. A series of samples was grown with nominal the same structure but different GaN contact layer thicknesses, which keeps the internal quantum efficiency constant while the extraction efficiencies are different. By scaling the calculated extraction efficiencies to fit the external quantum efficiencies determined by experiments, reliable extraction efficiencies are obtained.

Secondly, a procedure to determine the carrier density at various injection currents is developed. Recombination processes of electrons and holes in the quantum well(s) of LEDs strongly depend on the carrier density in the active region. It is necessary to obtain an reliable carrier density in the quantum wells for a better understanding of the recombination processes. The effects of p-n junction built-in electric field, piezoelectric field and screening of the electric fields caused by free carriers on the peak emission energy have been investigated. It is well known that the piezoelectric field causes an red-shift to the emission energy. The built-in electric field has the opposite sign to the piezoelectric field, which means that the built-in field and free carriers have a screening effect on the piezoelectric field. The screening is a function of carrier density. The dependence of emission energy on carrier density is calculated taken into consideration the p-n junction built-in electric field, the piezoelectric field and screening effect of free carriers. According to the calculation, there is a minimum of the emission energy for increasing carrier density. This is because the built-in electric field decreases and the screening caused by free carriers increases linearly and becomes dominant. A minimum of emission energy is indeed observed under electroluminescence condition when the current is varied from very low to high. Correct values for the carrier density are determined from comparing the minimum of the emission energy of simulation and measurement. For a specific sample the determination of the free carrier density was successful.

Thirdly, the dependence of the radiative lifetime and the nonradiative lifetime on carrier density is studied utilizing the above procedure. The radiative current density and nonradiative current density are calculated by separating the total current density via the internal quantum efficiency. For various currents the emission energy is measured and the corresponding carrier density is calculated and finally, the radiative lifetime and the nonradiative lifetime are derived. For the radiative recombination, the dependence of the lifetime on carrier density shows that the electric field affects the radiative recombination by reducing the overlap of electron and hole wavefunction in the quantum well. The non-radiative recombination is unclear. A strange behavior of the dependence of non-radiative lifetime on carrier density (non-radiative lifetime is not constant at lower carrier density region) is observed for some samples, which we cannot explain. More investigations and checks need to be carried out for those samples.

1. Introduction

The 2014 Nobel Prize for physics was awarded to Isamu Akasaki, Hiroshi Amano and Shuji Nakamura for the invention of super bright blue light emitting diodes (LEDs). The mechanism of light emission of light emitting diodes (LEDs) is electroluminescence (EL), converting electricity directly into photons of light, which is different from the traditional light source, e.g incandescent lamps rely on a heated filament to emit light, and fluorescent lamps generate light utilizing a gas discharge to excite phosphors. This property gives LEDs an advantage for achieving high efficiency. Using gallium nitride (GaN) based LED makes it possible that solid-state light (SSL) sources replace the traditional light sources. As SSL sources, GaN-based LEDs have several advantages over traditional lamps, including energy efficiency, robustness, long lifetime, and good thermal stability. It is currently estimated that approximately 261 TWh of electrical energy will be saved due to widespread use of white LEDs [1].

1.1. History of GaN-based LEDs

The first LED was invented by Henry Joseph Round in 1907 [2]. In the next nearly one century, LEDs are mostly used as indicator due to the absence of blue LED which is necessary for creating white light.

III-Nitride based materials are quite promising for blue emission due to their physical property, e.g. wide bandgap and direct band. Undoped III-Nitride crystals were typically highly n-type conductive. Therefore, the challenge is that p-type doping for III-Nitride was not achieved at that time. So the first blue and violet GaN-based LEDs were using the metal-insulator-semiconductor (MIS) structure (due to a lack of p-type GaN) by doping with Zn and Mg as a color center in 1971-1973 [3, 4]. The output power of the MIS LEDs was only of the order of 1-5μW. Akasaki and his co-workers at Meijo University demonstrated the first p-type doping in GaN using low-energy electron beam irradiation (LEEBI) treatment and the first p-n junction Gallium Nitride (GaN) LED In 1989 [5]. Two years later

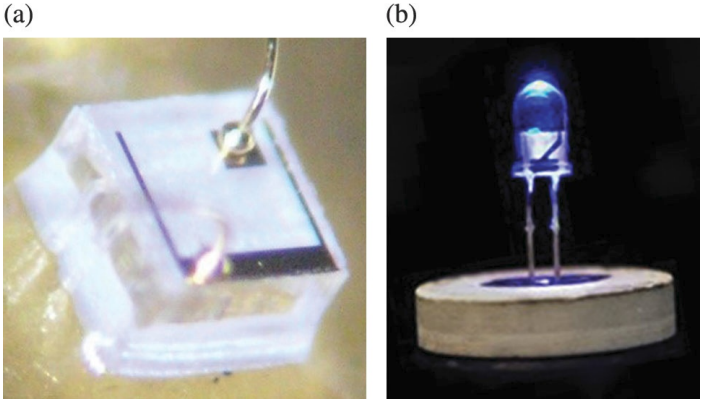

Figure 1.1.: (a) Image of a blue GaN LED with attached gold wire contacts (b) the same LED packaged as a commercial product [10].

in 1991, Nakamura et al. showed that Mg-doped GaN can also be activated by rapid thermal annealing at temperatures above 700°C in a N_2 atmosphere [6]. They also clarify the hole compensation mechanism as hydrogen passivation. A hydrogenation model wherein acceptor-hydrogen (H) complexes were formed in p-type GaN was proposed. Atomic hydrogen was produced by NH_3 dissociation during the growth [7]. The first high brightness p-GaN/n-InGaN/n-GaN DH blue LEDs were fabricated by Nakamura et al. in 1993[8]. The output power was 125 μW, the emission wavelength was 440 nm and the external quantum efficiency was as high as 0.22% at a forward current of 20 mA at room temperature. Due to a large lattice mismatch and thermal expansion coefficient difference between GaN and the sapphire substrate, a large number of threading dislocations (TDs) are generated from the interface between the substrate and the epilayer. GaN-based LEDs show surprisingly high power and efficiency. Commercially available blue LEDs with an output power of 1.5 mW, an external quantum efficiency of 2.7%, and the emission wavelength of 450 nm were demonstrated by Nakamura *et al.* in 1994 [9], as shown in Figure 1.1. Improvements have been made quickly. In 1995, Nakamura et al. demonstrated high-brightness LEDs for different wavelength: blue, green, and yellow with InGaN quantum-well (QW) structures [11]. Figure1.2 shows the epitaxial structure of green single quantum well (SQW) LED, which is still the basic foundation for all currently commercially available blue and green LEDs.

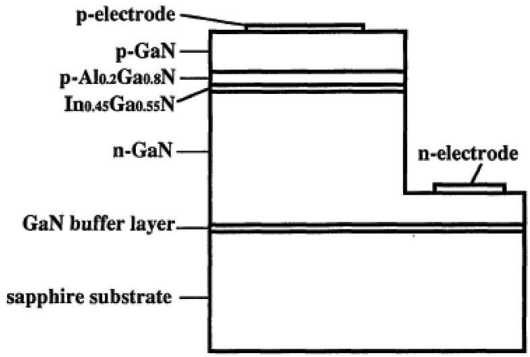

Figure 1.2.: Structure of a green single quantum well LED [10].

1.2. Current status and challenges for GaN-based LEDs

1.2.1. Green gap

Since 1995 Nakamura demonstrated GaN-based blue, green, and yellow LEDs, the external quantum efficiency were 7.3%, 2.1%, and 1.2% respectively [11], the efficiency of blue LEDs raised quickly beyond 80% [12], and green LEDs' efficiency also improved, with typical efficiency around 30% [13], but not as efficient as blue LEDs. GaN-based LEDs suffer from a dramatic decrease of efficiency with shifting peak emission wavelength from blue to green region, as shown in Figure 1.3. This is a well known phenomenon, the 'green gap' [11]. Usually the causes are attributed to two aspects: 1) poorer QW quality for the green LED due to the high indium content and low growth temperature of the green LED; 2) high piezoelectric field within QW caused by high indium concentration. [14]

1.2.2. Efficiency droop

Significant improvements have been achieved during the last decades since the first bright GaN-based blue LED was fabricated. One of the critical advantages of GaN-based LED lighting is its high efficiency compared to traditional lighting source. However, high efficiency occurs at low current density, such as only a few $A \cdot cm^{-2}$. LEDs' efficiency begin to decrease after reaching the maximum with further increasing driving current density, this

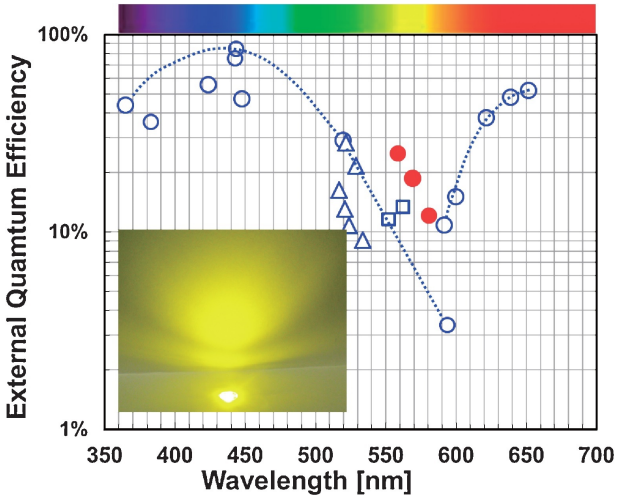

Figure 1.3.: Wavelength dependence of external quantum efficiency [13].

phenomenon is so called 'efficiency droop' [15], as illustrated in Figure 1.4. Such an efficiency droop behavior is a common phenomenon and observed for variable conditions: (1) across a broad wavelength spectrum of GaN-based LEDs from deep ultraviolet to yellow [16, 17, 18, 19], (2) also takes place under pulsed current operation at duty cycles and pulse widths for which thermal effects can be ruled out as a cause for the efficiency decay [20, 21], (3) in both resonant photoluminescence (PL) and electroluminescence (EL) measurements with very similar excitation dependences [22, 23], (4) polar, non-polar,and semi-polar QW LED structures also suffer from the droop problem [24, 25, 26, 27]. On the one hand, the efficiency droop has become the major obstacle for realization of high power LEDs which require high current density. On the other hand, from the scientific standpoint, the underlying physical mechanism for the droop phenomenon is currently still not fully understood.

1.3. Possible mechanisms for efficiency droop

In order to understand and eliminate the efficiency droop, despite having been the subject of extensive research efforts for a decade, the physical origin of droop has not been clarified. Many different contributions to efficiency droop have been proposed and discussed: Auger

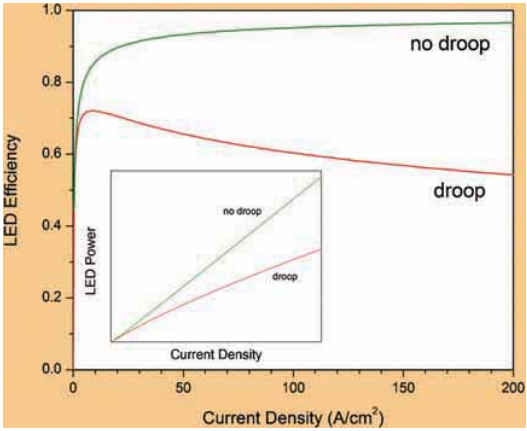

Figure 1.4.: Illustration of LED efficiency droop [28].

recombination [29, 30, 31, 32], defect-related nonradiative recombination [33], electron leakage hole injection efficiency [34, 35], carrier delocalization effects [36, 37, 38]. Actually all the possible mechanism can currently be attributed to two aspects: either carrier-density-dependent nonradiative recombination or carrier leakage. Obviously, the carrier density in the QW in LED is a crucial parameter to understand the recombination process. However, a key problem of earlier studies on loss mechanism is that there is no direction access to the carrier density, especially for LED, but only via a popular ABC model (see equation 5.1) which is too simple to offer the complete information about the recombination processes in the QW.

1.3.1. Carrier density dependent nonradiative recombination

Auger recombination is the most straightforward nonradiative recombination process at high carrier density and one of the most debated droop mechanisms. This process involves three particles: an electron from the conduction band recombines with a hole in the valence band with transferring the energy to a third electron (or hole). Lots of efforts to verify the Auger recombination have been carried out both theoretically and experimentally. Hader et al. computed a very small Auger coefficient C of 3.5×10^{-34} cm^6/s using the $8\times8\ \vec{k}\cdot\vec{p}$ band model for the direct band-to-band Auger process and concluded that this value is too small to explain the experimentally observed droop [23]. Delaney et al. calculated a peak

Auger coefficient of 2×10^{-33} cm^6/s in bulk InGaN with a 2.5 eV bandgap (λ_g =495 nm) using first-principle density-functional and many-body-perturbation theory and argue that an interband Auger may be responsible for droop in InGaN LEDs [39]. Several attempts to measure Auger coefficient C experimentally have been reported and different C value have been obtained [22, 29, 40, 41, 42, 43]. These conflicting results indicate that the controversy on Auger recombination for GaN-based LED is far from being settled.

Besides Auger recombination, defect-related nonradiative recombination is another possible cause depending on carrier density. InGaN/GaN QW LED structures have lots of defects compared to other III-V semiconductors. Since the early stage, much attention has been paid to the defect-related recombination mechanisms as another origin of the efficiency droop [33, 44, 45, 46, 47]. Additional increase of nonradiative recombination rate due to defect-related nonradiative recombination mechanisms in the MQW active region cannot fully explain the temperature dependent characteristics of the efficiency droop [24, 48]. The key problem of earlier studies is the missing direct access to carrier density, only via ABC model.

1.3.2. Carrier leakage

As another possible contribution to the droop, a carrier leakage model was proposed to explain this phenomenon in 440 nm (blue) InGaN/GaN LEDs having different dislocation densities. A rate equation model was developed to describe the competition between monomolecular nonradiative recombination, radiative recombination, and an additional recombination term that dominates at high currents [49]. Given the different physical origins that can cause carrier leakage, this mechanism can be subdivided into leakage caused by ineffective confinement of carriers in the QWs, poor injection and distribution of holes, and Auger-assisted electron overflow. Experiments have been performed to investigate the effects of carrier leakage [50, 51, 52]. It seems that carrier leakage indeed contributes to the droop. However, carrier leakage is more likely one of droop causes rather than a single mechanism.

2. Crystal structure and physical properties of III-nitrides

In this chapter the crystal structure and physical properties of III-nitrides will be introduced as basic background knowledge. We will then discuss spontaneous polarization and piezoelectric polarization.

2.1. Crystal and band structure of group III-nitrides

Group III-nitrides (AlN, GaN and InN) have three kinds of crystal structures: the hexagonal wurtzite structure, the cubic zincblende structure, and the rocksalt or NaCl structure [53]. The zincblende structure for GaN and InN has been stabilized by epitaxial growth of thin films on the (001) crystal planes of cubic substrates, such as Si, MgO, and GaAs, while for AlN no stable zincblende phase has yet been found. The rocksalt or NaCl structure can be obtained at very high temperature. The wurtzite structure is the thermodynamically stable structure for AlN, GaN, and InN at ambient conditions, which are also the most common structures because they are the easiest to grow and had given best results for optoelectronic applications.

Almost all of the research focus on wurtzite structure is due to its advantages regarding growth and physical properties. Our concern is also the wurtzite structure, so we only introduce the wurtzite structure. An illustration of the wurtzite structure is shown in Figure 2.1, where nitrogen atoms form a hexagonal close packed structure (HCP) and half of the tetrahedral sites are occupied by group III elements in the HCP lattice. Each nitrogen atom is coordinated by four group III atoms, conversely, each group III atom is coordinated by four nitrogen atoms. The arrangement of the nitrides can be viewed as containing hexagonal double layers, the two layers are occupied by nitrogen and Group III elements respectively. The wurtzite structure is non-centrosymetric, which leads to a unique axis perpendicular to the hexagons along the 0001 direction, usually labeled as c direction. For the wurtzite

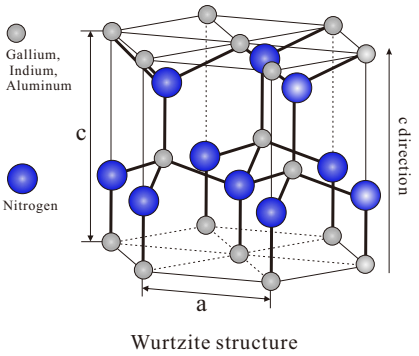

Figure 2.1.: Illustration of hexagonal wurtzite structure.

Parameter	AlN	GaN	InN
Lattice constant a_0 (Å)	3.111	3.189	3.538
Lattice constant c_0 (Å)	4.980	5.185	5.704
Melting temperature (K)	3487	2791	2146

Table 2.1.: Physical property of group III-Nitrides [54, 55, 56, 53].

structure, the stacking sequence of (0001) planes is ABABAB along the c direction. Group III-nitrides are polar crystals because of the absence of a center of inversion symmetry along the c-axis. Table 2.1 gives the parameters for lattice Gallium Nitride (GaN) and the other compounds of III-nitrides.

The optical and electronic properties of semiconductor material are mainly determined by its band structure. There are numerous publications in which the band structure of the Group III nitrides have been calculated using different methods. Figure 2.2 shows Goano et al. calculated band structure of the wurtzite GaN [57]. It can be seen that both the minimum of the conduction band and the maximum of valence band are located at the Γ-point in the center of the first Brillouin zone. Figure 2.3 shows the bandgap of wurtzite GaN near the Γ-point. The band structures of all the group-III nitrides have direct band gaps at the center of the Brillouin zone (Γ-point).

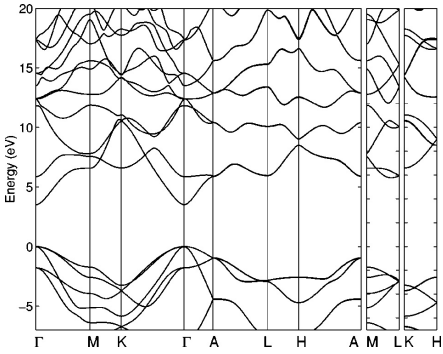

Figure 2.2.: Calculated band structure of wurtzite GaN[57].

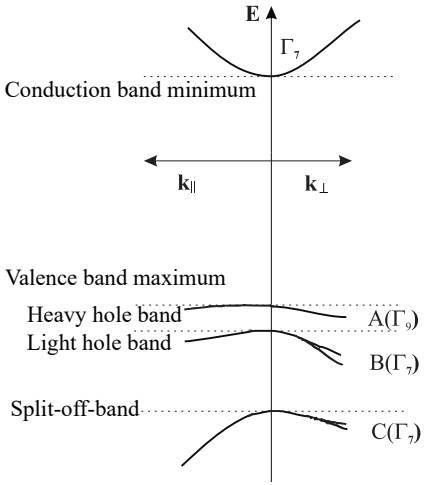

Figure 2.3.: Band structure of GaN at the Γ point in the center of Brillouin zone.

Parameter	GaN	InN
E_g (4 K)	3.51 eV [55]	0.67 eV [56]
E_g (300 K)	3.43 eV [55]	0.61 eV [56]
m_e/m_0	0.2 [59, 62]	0.07 [63]
m_h/m_0	2.0 [59, 62]	0.4 [63]

Table 2.2.: Band gap energy and effective mass for GaN and InN.

Table 2.2 shows the effective mass of wurtzite GaN. While the electron mass has been measured by direct cyclotron resonance experiments, which gives a value of m_e= $0.22m_0$ [58], the value of the hole effective mass is so far uncertain. Based on absorption and lifetime measurements, effective hole vaule, $2.2m_0$ has been estimated [59], which is slightly higher than the theoretical value [60, 61]. In this work, the value of $m_h = 2m_0$ was applied to theoretical calculations [59, 62].

The band gap energy of a ternary alloy such as GaInN is given by the composition-weighted average of the GaN and InN band gaps including a non-linear term described by the bowing parameter b:

$$E_{g,Ga_{1-x}In_xN} = (1-x)\cdot E_{g,GaN} + x\cdot E_{g,InN} - x\cdot(1-x)\cdot b_{GaInN}, \tag{2.1}$$

where x is the molar fraction of Indium. Several bowing parameters for $Ga_{1-x}In_xN$ are reported: b=1.4eV[64], b=2.5 eV[65], and b=0.97eV[66]. The value of 1.4eV reported by Wu et al is the commonly accepted value.

2.2. Polarization field of the group III-nitride semiconductors

Usually, for group III-nitrides of wurtzite structure the common epitaxial growth direction is along the c direction. Due to the property of non-centrosymetric of polar crystals, there are polarization charges located at each of the two surfaces of a layer, which is so called spontaneous polarization. The direction of spontaneous polarization for wurtzite AlN, GaN and InN is along c-axis and opposite to the [0001]. Vegard-like rule can be used to estimate the spontaneous polarization.

For the III-nitrides heterostructure, large mismatch of lattice constant between different layers result in mechanical stress which also cause polarization, namely piezoelectric po-

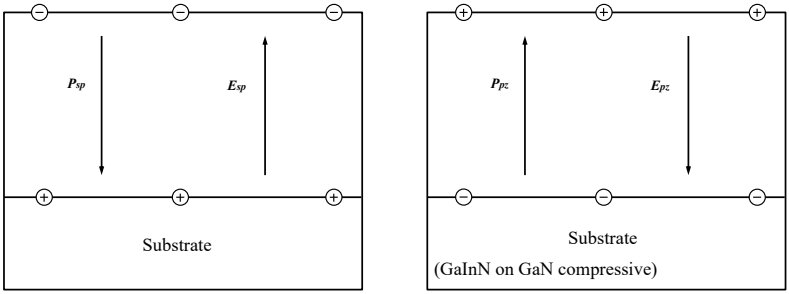

Figure 2.4.: Piezoelectric polarization field.

larization. The piezoelectric polarization P_z can be determined by the following equation [67]:

$$P_z = 2d_{31}(c_{11} + c_{12} - \frac{2c_{13}^2}{c_{33}})\varepsilon_{xx}, \tag{2.2}$$

where d_{31} is the is the relevant piezoelectric tensor component, c_{ij} are the elastic constants, and ε_{xx} is the in-plane strain. In the general case, both of spontaneous polarization and piezoelectric polarization contribute to the total polarization P_{total},

$$P_{total} = P_{sp} + P_{pz}(\varepsilon), \tag{2.3}$$

where P_{sp} and $P_{pz}(\varepsilon)$ is the spontaneous polarization and piezoelectric polarization, respectively. Figure 2.4 shows illustration of the spontaneous and piezoelectric polarization and the static electric field caused by polarizations for the cases of common GaInN/GaN QWs. We can see that the direction of spontaneous polarization and piezoelectric polarization is opposite.

The difference in spontaneous polarization between GaN and InN is rather small compared to the piezoelectric polarization due to the large lattice mismatch between GaN and InN. Thus, in many cases for GaInN/GaN QWs, contribution from the spontaneous polarization to the total polarization are negligible compared to the piezoelectric polarization. Several methods have been proposed to experimentally estimate the piezoelectric polarization [68, 69]. The internal electric field induced by piezoelectric polarization is

$$F_{pz} = -\frac{P_z}{\varepsilon_0 \varepsilon_r}, \tag{2.4}$$

where ε_0 and ε_r are the absolute dielectric constant and relative dielectric constant respectively. The direction of piezoelectric field is opposite to the c direction and from p-GaN to n-GaN for the case of LEDs with GaInN/GaN QWs.

3. Calculation of extraction efficiency and experimental calibration

The determination of a reliable internal quantum efficiency (IQE) is a key step to understand the physical mechanism of the efficiency droop. Temperature-dependent variable-excitation photoluminescence (PL) [70, 71] and temperature-dependent electroluminescence (EL) [72, 73] are the experimental methods most widely used for estimation of IQE. Both techniques are based on intuitive assumptions that non-radiative recombination can be eliminated or neglected at low temperatures, providing nearly 100% IQE. However, it was experimentally verified that these mechanisms are still present at low temperatures [74]. As an alternative way, the IQE can be calculated from measured external quantum efficiency if the extraction efficiency can be determined without these assumptions.

In this chapter an optical determination of the IQE via a calculation of the extraction efficiency and its calibration with measured data will be introduced. First, we will introduce the concepts of all kinds of efficiencies and their relationship. Then the structure of our LED samples will be illustrated, which is the basis of our calculation of the extraction efficiency. The theories and processes of calculation of extraction efficiency will be discussed. Finally, our theoretical result was calibrated with experimental data to obtain a reliable extraction efficiency.

3.1. External quantum efficiency, Internal quantum efficiency and Extraction efficiency

In order to illustrate the efficiencies related to GaN-based LEDs, a simplified common LED's structure is shown in Figure 3.1. The first layer is the substrate which can be GaN, sapphire, SiC or Si. Sapphire is used by most of the commercial LEDs due to its more suitable physical properties and high price performance ratio compared to others. Usually the second layer is un-doped GaN grown as a buffer layer. Then a n-type GaN layer is

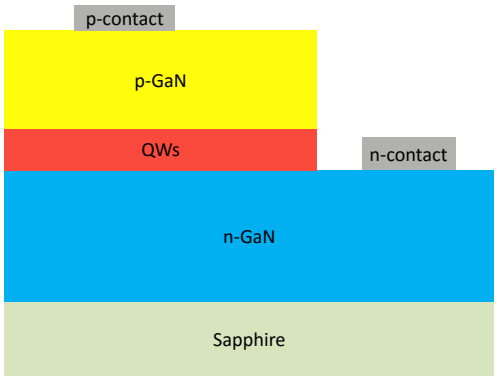

Figure 3.1.: Illustration of typical structure of LED.

grown with Si doped as donors. The following layers are InGaN/GaN QWs and then there will be a thin AlGaN layer used as electron blocking layer (EBL). The last layer is p-type GaN which provides the holes. When applying forward voltage on p-contact and n-contact, electrons from n-type GaN and holes from p-type GaN will be injected to the active region (QWs) respectively. Electrons and holes will recombine within the active region by emitting photons. In the ideal case, all the electrons and holes should be injected into active region and recombination radiatively. However, under the practical conditions, some of the electrons and holes can not be captured by the active region. The injection efficiency η_{inj} is defined as the ratio of electrons (holes) injected into active region to the total electrons (holes) from the n-layer (p-layer).

$$\eta_{inj} = \frac{numbers\ of\ electrons\ captured\ by\ active\ region}{numbers\ of\ total\ electrical\ injected\ electrons}. \tag{3.1}$$

Electrons and holes injected into the active region will recombine. There are three forms of recombination for the electrons and holes. Due to the defects in the active region, which will form recombination centers, some electron and hole pairs recombine in the recombination center without emitting photons. Also, a fraction of electron-hole pairs can recombine by emitting a photon which is the desired case. Electrons and holes can also recombine and pass the energy to a nearby electron or hole, which is called Auger recombination. Both defect-related recombination and Auger recombination is unwanted because the results of the two recombination processes is generating heat rather than photons. The internal quantum efficiency (IQE) is defined as the ratio of electrons (holes) recombining radiatively to

the total electrons (holes) within the active region, which is also called radiative efficiency:

$$\eta_{IQE} = \frac{number\ of\ photons\ generated}{number\ of\ electron-hole\ pairs}. \tag{3.2}$$

GaN has a higher refractive index which causes total internal reflection at the interface of GaN and air. As a result not all the photons emitted from active region can escape from the LED to free space. The extraction efficiency (EXE) is defined as the ratio of photons coming out to the air divided by the total number of photons generated by the active region. Usually the extraction efficiency is mainly determined by the LED architecture (such as shape of the chip [75], use of patterned substrates [76], photonic crystals [77], surface roughening [78, 79], etc.), with however some dependence on materials parameters (absorption and reflection of materials, etc.) and peak emission wavelength of LED.

$$\eta_{EXE} = \frac{number\ of\ photons\ coming\ out}{all\ photons\ generated}. \tag{3.3}$$

The external quantum efficiency (EQE) is the ratio of the number of photon emitted to free space to the electrons comprising the current through the LED.

$$\eta_{EQE} = \frac{number\ of\ photons\ coming\ out}{number\ of\ injected\ electrons} = \frac{P_{out}/(h\nu)}{I/e}, \tag{3.4}$$

where P_{out} is the light output power, h is Planck's constant, ν is the light frequency, $h\nu$ is the photon energy, I is the injection current, e is the elementary charge. According to Eq 3.4, the EQE then can be calculated easily by measuring the light output power P_{out}, the injected current I and the peak emission energy of the LED. According to the definition of IQE, extraction efficiency, and EQE, their relation can be derived as follows

$$\eta_{EQE} = \eta_{inj} \cdot \eta_{IQE} \cdot \eta_{EXE}, \tag{3.5}$$

where η_{inj} is usually assumed unity. The wall-plug efficiency is defined as the ratio of emitted light output power to the electrical input power.

$$\eta_{Wall-plug} = \frac{P_{out}}{IV}, \tag{3.6}$$

where V is the applied forward voltage, IV is the electrical power provided to the LED

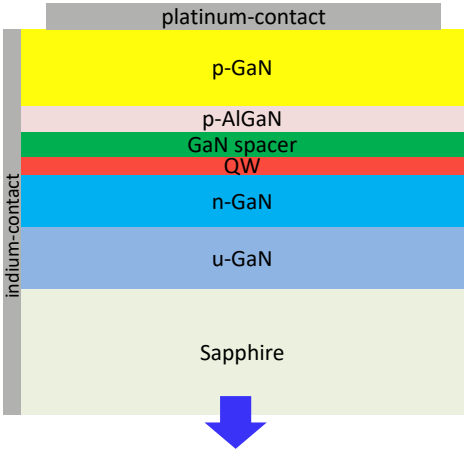

Figure 3.2.: Structure of our LED samples.

3.2. Growth and structure of GaN-based LED sample

Our LED samples were grown by low pressure metalorganic vapour phase epitaxy (MOVPE), using a horizontal reactor (Aixtron AIX 200RF). Double-side polished c-plane sapphire ($\alpha-Al_2O_3$) was used as the substrate for the purpose of a quantitative calculation. First about 25nm of undoped GaN nucleation layer was deposited on the substrate for the purpose of improving the crystal quality of the upper layers. There is also about 2 μm undoped GaN. Then the following layer is a 2 μm n-GaN layer doped with silicon, with a doping concentrationof $5\times10^{18}\cdot cm^{-3}$. Before the QW layer is a highly n-doped GaN in order to obtain a high quality QW. A $Ga_xIn_{1-x}N$ single QW (SQW) with thickness of 2.5nm were grown followed by a GaN (barrier) spacer layer. P-type $Al_xGa_{1-x}N$ with thickness 10nm was used as electron blocking layer. The last layer is p-type GaN doped with Magnesium with a thickness of 110nm. Platinum with a diameter of 450 μm was deposited on the p-GaN as the p-contact. The whole growth process is based on our former optimization for GaInN SQW structure green LEDs [80]. The thickness and composition for different layers are characterized by high resolution X-ray Diffraction (XRD) by Dr. Heiko Bremers. Fig 3.2 shows the structure of our LED samples. We use double polished sapphire as substrate. So the sample is transparent. Fig 3.3 shows the picture of our sample. Platinum is deposition on the p-GaN as the p-contact which also plays a role of metallic mirror to

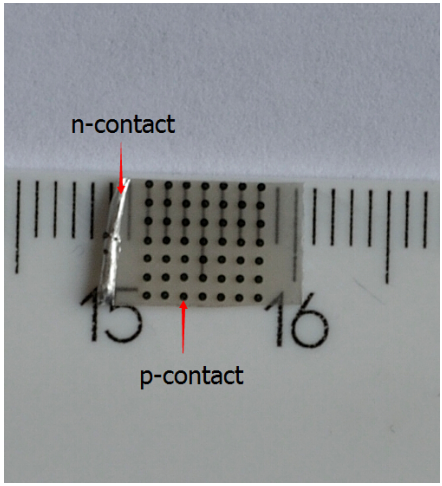

Figure 3.3.: Sampe of SQW blue LED.

reflect the light emitted from the QW. For the n-contact, we use indium at the lateral side of the sample. The indium will connect with the p-GaN layer as well, however, the current through indium to p-contact is rather small and negligible compared to the forward current through the QW under forward voltage condition due to the high resistance of p-GaN and a poor contact between indium and p-GaN.

3.3. Calculation of the extraction efficiency

3.3.1. Theory of light propagation

When light propagates through the interface between two different media, part of it will be reflected, and part of it will be transmitted (or refracted) into the new medium. As shown in Fig 3.4, the angle of reflection will be the same as the angle of incidence, while the angle of refraction follows a more complicated law named the Snell-Descartes law, as following

$$\frac{\sin\theta_1}{\sin\theta_2} = \frac{v_1}{v_2} = \frac{n_2}{n_1}, \tag{3.7}$$

where v_1 and v_2 are the velocity of light in the medium I and II, n_1 and n_2 are the refractive indices of the different medium I and II, respectively. According to Eq 3.7, if the refractive

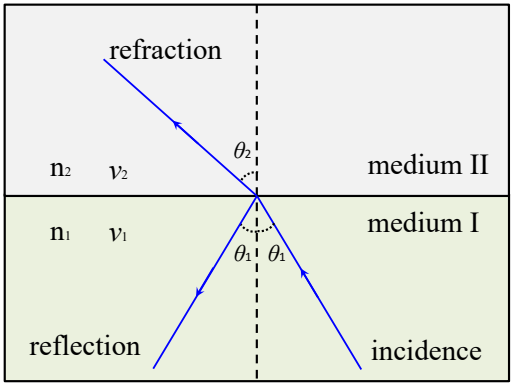

Figure 3.4.: Propagation of light through two different media.

index n_2 of the medium I is higher than that of the medium II, n_1, there will be an effect referred to as total internal reflection (TIR) for the incident light beyond a certain angle, the light is entirely reflected at the interface, and no light is transmitted. This certain angle is called critical angle, which can be determined by Eq 3.7 when θ_2 equals 90°

$$\theta_{critial} = \arcsin(\frac{n_2}{n_1}\sin\theta_2) = \arcsin\frac{n_2}{n_1}. \tag{3.8}$$

Regarding to GaN-based LEDs, which tend to have low extraction efficiency, largely due to the high index of refraction of GaN (n≈2.5). This high value means a small critical angle ($\theta_{critial}$ ≈23.6°) and a small fraction of emitted light can escape from the LED if there is no optimized structure.

When the light go through different media, the reflected and refracted amplitudes are described by the Fresnel formulae [81]:

$$T_{\parallel} = \frac{2n_1\cos\theta_1}{n_2\cos\theta_1 + n_1\cos\theta_2}A_{\parallel} \tag{3.9a}$$

$$T_{\perp} = \frac{2n_1\cos\theta_1}{n_1\cos\theta_1 + n_2\cos\theta_2}A_{\perp} \tag{3.9b}$$

$$R_{\parallel} = \frac{n_2\cos\theta_1 - n_1\cos\theta_2}{n_2\cos\theta_1 + n_1\cos\theta_t}A_{\parallel} \tag{3.9c}$$

$$R_{\perp} = \frac{n_1\cos\theta_1 - n_2\cos\theta_2}{n_1\cos\theta_1 + n_2\cos\theta_t}A_{\perp} \tag{3.9d}$$

where T and R are the complex amplitudes of the transmitted and reflected light waves, respectively. A is the amplitude of the electric vector of the incident light.

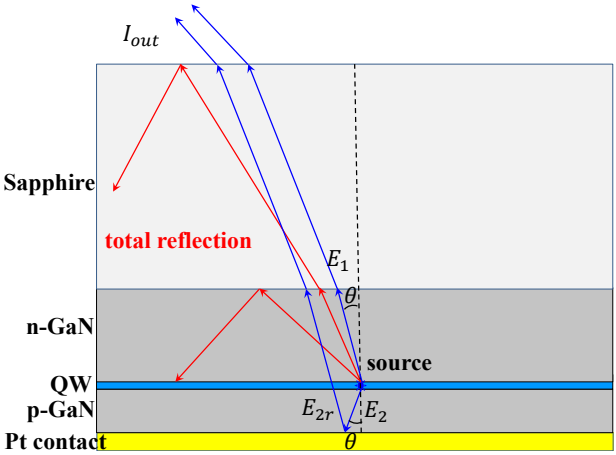

Figure 3.5.: Light path in the sample.

3.3.2. Calculation of the extraction efficiency for our LEDs

According to the definition of the extraction efficiency Eq 3.3, in principle we need to count the number of photons escaping from LED and number of photons emitting from active region, which is impossible technically. While, since the intensity of light is proportional to the number of photon we can obtain the extraction efficiency if we can calculate the ratio of intensity of escaped light to the total emitted light intensity. For an individual light ray, the transmission of light going through different layers follow the Fresnel Eq 3.9. Considering the effect of total internal reflection and the critical angle $\theta_{critical}$ for the GaN-based LED, then the extraction efficiency should be the integration of the intensity of every single light ray:

$$\eta_{EXE} = \frac{\int_0^{\theta_{critical}} I_{out}(\theta) d\theta}{\int_0^{2\pi} I_o(\theta) d\theta}, \tag{3.10}$$

where $I_{out}(\theta)$ is the intensity of a single beam of light coming out for a specific incident angle θ, $I_o(\theta)$ is the corresponded intensity of the original light. The relationship between $I_{out}(\theta)$ and $I_o(\theta)$ follows the Fresnel Eq 3.9, which depends on incident angle θ, refractive index of GaN and sapphire and wavelength.

Fig 3.5 illustrates the light path in our LED sample. Light emitted from GaInN/GaN QW goes into the upper (n-type) GaN and the lower (p-type) GaN layers. Since the GaN has

a higher refractive index than that of sapphire, there will be total reflection when the light goes through the interface of GaN and sapphire. There will be also total reflection at the interface of sapphire and air due to higher refractive index of sapphire than air. Both cases are shown as the red ray in Fig 3.5. Only the light which have the incident angle smaller than $\theta_{critical}$ can reach air. The blue rays show the light which can escape from LED structure. The upper part E_1 go through n-GaN and sapphire and reach air. The down part of the light will be reflected at the interface between metallic mirror (Platinum contact), like E_2 and E_{2r}. E_1 and E_2 have the same incident angle. As a consequence, the light rays which can reach the air are the results of interference of $E_1$and E_{2r}, E_{2r} is the light reflected by the metallic contact mirror and parallel with E_1. Then we can calculate the intensity for a specific light ray,

$$I = I_1 + I_{2r} + 2\sqrt{I_1 I_{2r}}\cos\delta, \tag{3.11}$$

where I_1 and I_{2r} is the intensity of the light E_1 and E_{2r}. E_{2r} is the reflection part (reflected by metallic mirror) and is parallel to E_1, as shown in Fige 3.6. δ is phase shift, which is determined by two contributions:

$$\delta = \delta_{\Delta L} + \delta_r, \tag{3.12}$$

where $\delta_{\Delta L}$ is the phase shift due to the optical path length differences, and δ_r is the phase shift upon reflection off the metallic mirror, namely phase shift between E_{2r} and E_2. δ_r can be calculated using the optical constants of the metal [81]. In order to calculate the intensity of interference of E_1 and E_{2r} ,we also have to know the their path difference which depends on the cap thickness and angle of emergence. According to Fig 3.6 the path difference is determined by the following function:

$$\Delta L = \frac{d}{\cos\theta}(1 + \cos 2\theta), \tag{3.13}$$

where ΔL is the path difference, d is the cap thickness which can be measured by XRD, and θ is incident angle.

With Eq 3.9, 3.10, 3.11, 3.12 and 3.13, assuming the interfaces between different layers are ideal, we can obtain the extractin efficiency depending on cap thickness for different wavelength. Fig 3.7 shows the result of calculation of the ideal extraction efficiency. We can see that the extraction efficiency depends on the cap thickness and the peak wavelength. The extraction efficiency without optimizing LED structure is rather low, the maximum is only about 16% because most of the emitted light can not escape due to total internal reflection.

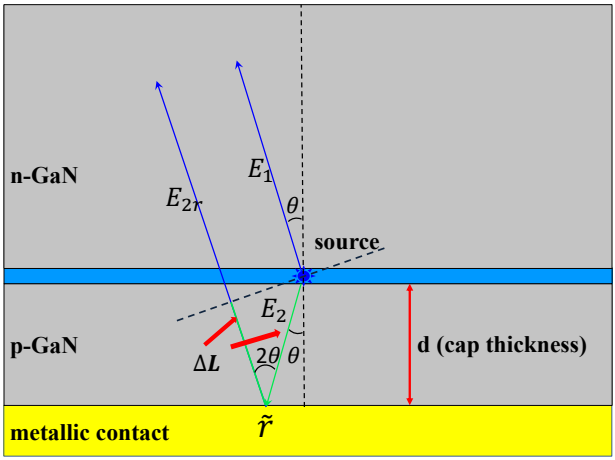

Figure 3.6.: Light path at the interface of metal-sapphire in the sample.

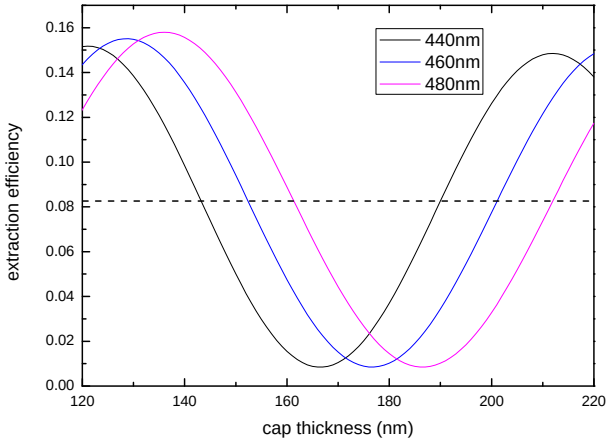

Figure 3.7.: Ideal extraction efficiency for different peak wavelength.

Sample	Cap thickness (nm)
BS2345	162
BS2346	136
BS2347	190
BS2348	151
BS2349	177
BS2355	197

Table 3.1.: Cap thickness for different LED samples determined by XRD by Dr. Heiko Bremers.

3.4. Calibration of extraction efficiency with experimental results

We need to calibrate our calculated extraction efficiency with experimental results in order to obtain the real extraction efficiency because during our calculation processes several conditions are assumed to be ideal case, for example, ideal layer thickness, ideal sharp interface, and ideal flat interface, etc.

3.4.1. Experimental methods

We grew six samples which have nominally the same structure except for a variation of the cap thickness, which means all the samples should have the same internal quantum efficiency and peak emission wavelength. The cap thickness for different samples is shown in Table 3.1. According to the definition of the extraction efficiency, the extraction efficiency for different samples will vary with a change of the sample structure, namely the cap thickness. Given the relationship between IQE, EQE and the extraction efficiency, as shown in Eq 3.5, the EQE depends on variation of extraction efficiency if the IQE is constant. The EQE can be calculated easily by the measured parameters.

We measured the light output power, voltage, current and peak wavelength under electroluminescence (EL) condition for our samples. Figure 3.8 shows the spectra of our LED sample under EL condition at 20mA. The peak emission wavelength is λ_{peak} =454nm, for sample BS2349 and BS2355, λ_{peak} =459nm for sample BS2346, BS2347 and BS2348, λ_{peak} =468nm for sample BS2345, respectively. The peak emission wavelength is not exactly same even though all the samples have nominally the same QW structure and Indium concentration. The most likely reason is a fluctuation of indium composition and

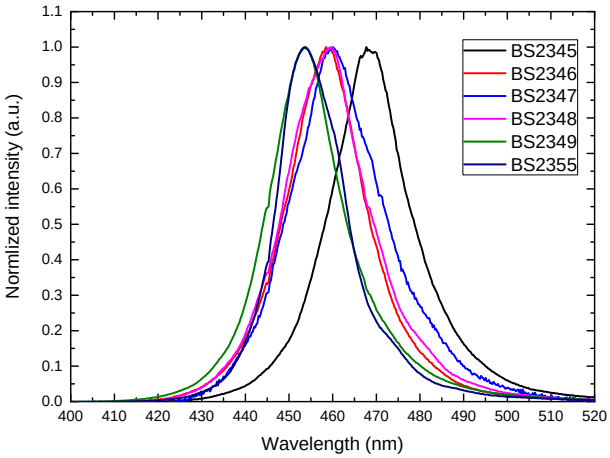

Figure 3.8.: Emission wavelength for different SQW blue LED at 20mA.

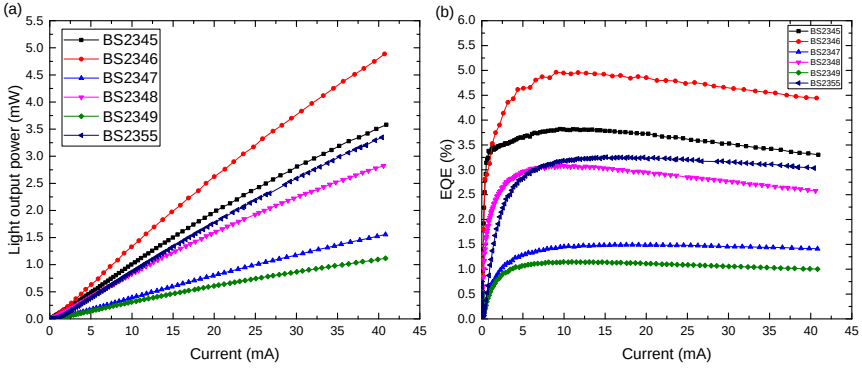

Figure 3.9.: Dependence of light output power(a) and EQE(a) on current.

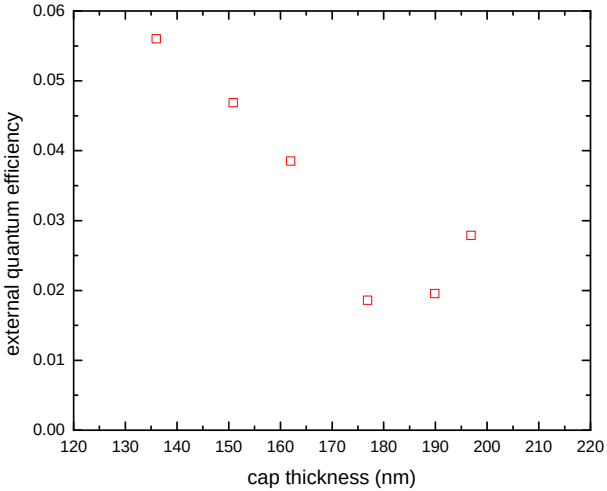

Figure 3.10.: External quantum efficiency depends on cap thickness.

QW thickness. We also notice that the peak wavelength increases with the increase of the growth sequence number. The reason for this phenomenon is still unknown. We calculated the EQE at 20mA for all the samples according to Eq 3.4. Figure 3.9 show the dependence of the light output power and EQE on current. We can see that these samples show quite different behavior which is mainly caused by the different cap thickness. The range of light output power is from 0.61mW to 2.62mW for different samples at 20mA, as shown in Figure 3.9(a). Obviously the droop phenomenon for the EQE is observed from Figure 3.9(b), and the EQE reaches the maximum at a current between 5mA to 10mA. We did not have any optimization processes for improving light extraction for our LED samples, which results in rather low extraction efficiency, so the maximum EQE of our samples is only about 5%.

3.4.2. Calibration process

Fig 3.10 shows the EQE at 20mA. Since we can determine the EQE experimentally and we also already have the relationship between EQE and IQE. All the samples have the nominally same IQE, which means the IQE should be constant for our different samples. It is obvious that the variation of the EQE is caused by the change of extraction efficiency due

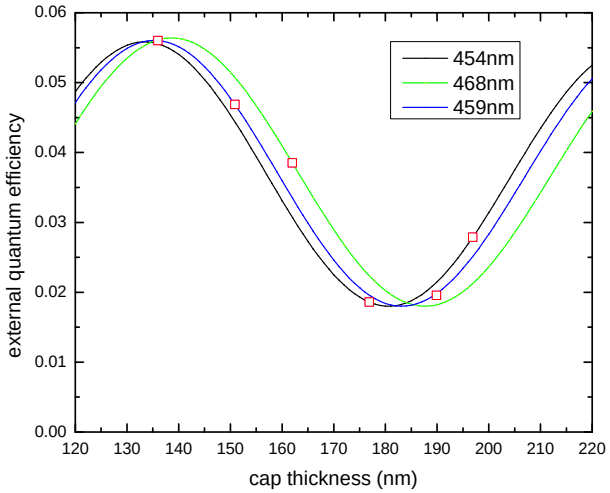

Figure 3.11.: Calibration of ideal extraction efficiency with measured EQE.

to the different cap thickness.

First we take into account the correct emission wavelength for each LED. Then for the light ray E_{2r} we need to reduced effective reflectivity due to interface roughness of metallic mirror. The phase shift also need to be adjusted because the possible effect of an oxide interlayer might influence the phase during reflection of light. Here we use the follow equation to fit our calculation to the measured EQE,

$$\eta_{EQE} = \eta_{IQE} \cdot e^{R_{number}} \cdot \eta_{EXE}(d, \lambda), \tag{3.14}$$

Considering that IQE of LED degrades with runs of grow sequence number even keeping growth parameters same, we introduce an exponential coefficient $e^{R_{number}}$ which is an experiential parameter. By adjusting the IQE, the reflectivity and phase shift, we are able to fit our calculation to the experimental results every well, as shown in Figure 3.11. Then we can get the extraction efficiency for a specific sample. The calculation and calibration make us obtain more reliable IQE, which is based on the experiments not some assumptions, e.g. assuming IQE is unite for PL at low temperature. We can apply the fitted parameters (reflectivity and phase shift) to other samples which have the same metal contact condition to calculated extraction efficiency.

Fig 3.12 shows the comparison of ideal extraction efficiency and the scaled extraction effi-

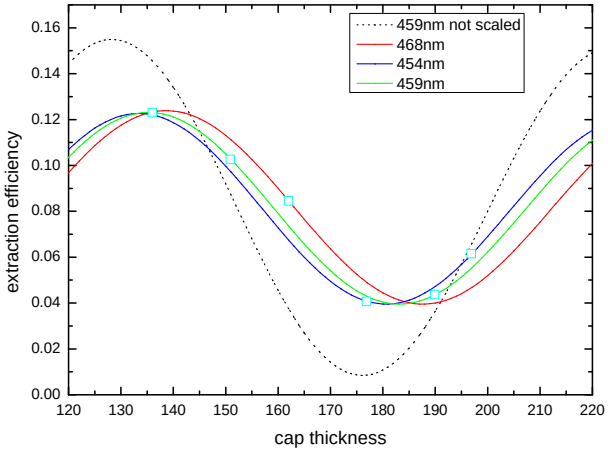

Figure 3.12.: Comparision of extraction efficiency with and without calibration.

ciency. We can see that the actual extraction efficiency have some apparent 'shrink' compared to the calculation results. The main reason might be the poor reflection of the interface between GaN and metal due to the rough surface of the metal mirror.

Figure 3.13 shows the real IQE of our samples. We can observe that there is an obvious degradation of IQE with increase of growth sequence number. The reason is still not clear. One of the possible causes might be the accumulation of Magnesium in the reactor which might impact the IQE of the QW. The red data in Figure 3.13 comes from the sample that was not in the same sequence of other samples. We can see that the degradation is eliminated.

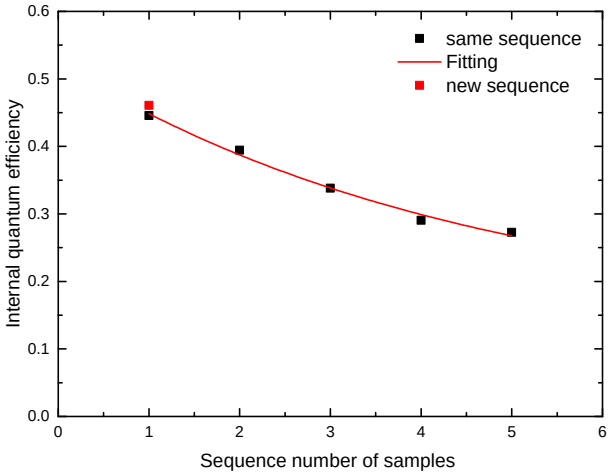

Figure 3.13.: Real IQE dependence on sample number.

4. Determination of the carrier density

In order to understand the recombination processes of the electrons and holes in the QW in an LED, it is vital to find out the carrier density in the QW. In this chapter, we will discuss how the total electric field F_{total} , which includes the piezoelectric field, electric field of free carriers and built-in electric field of p-n junction, in QW affect the emission wavelength λ. Then the carrier density can be determined via the relationship between F_{total} and the peak emission energy compared to the experimentally measured peak emission energy.

4.1. Electric field in a QW of a LED

Electric fields in the QW of a LED have strong effects on its optical properties and recombination so in order to determine the carrier density we need to figure out the electric field first. The polarization field and its screening by free carriers in the QW play an important role as two well-known factors. Besides that, the built-in electric field caused by the net charge in the depletion region also needs to be considered since a LED with a single QW is actually a p-n junction.

4.1.1. Polarization field effect in QW: Quantum-confined Stark effect

As our samples are typical LEDs grown on c-plane GaN which has a strong polarization along the c-direction, the polarization field in the GaInN/GaN QW must be considered. The quantum-confined Stark effect (QCSE) was first reported by Miller *et al*. in the context of the GaAs/AlGaAs quantum well (QW) structures with an electric field applied perpendicular to the layers [82]. Tetsuya Takeuchi et al. studied the influence of the piezoelectric fields on luminescence properties of GaInN strained quantum wells [69]. They reported that the electric field, as high as 1.08 MV/cm, is induced by the piezoelectric effect in strained $Ga_{0.87}In_{0.13}N$ grown on GaN. Figure 4.1 illustrates the QCSE. First, the piezoelectric field tilts the band structure of the QW which can result in a narrowing of the effective bandgap.

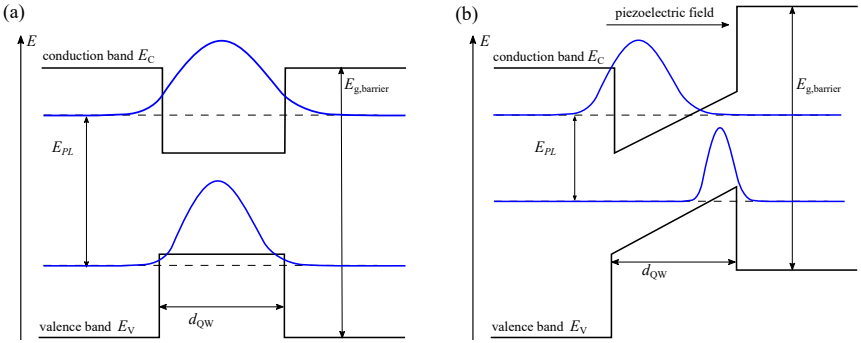

Figure 4.1.: QW band structure (a), influence of piezoelectric field: QCSE (b).

A red-shift of emission energy will be caused by the QCSE. It will also cause a spatial separation of electrons and holes wave function within the QW, as shown in Figure 4.1(b). The separation of electron and hole wave functions can reduce their recombination probability and decrease the IQE [83].

Utilizing the QCSE, a method of experimental determination of the internal polarization field in GaInN/GaN quantum wells has been developed [68]. Figure 4.2 shows the dependence of internal field on the Indium mole fraction. With this method we are able to calculate the piezoelectric field for our samples according to the Indium composition determined by XRD in the QW.

4.1.2. Electric field of free carriers

With increasing injected carrier density in the QW, the electric field caused by carriers, which has the opposite sign of the polarization field, will produce an effect of screening the piezoelectric field. A blue-shift of the peak emission wavelength has been observed for both photoluminescence (PL) with increasing excitation intensity [69] and electroluminescence (EL) with increasing current [84, 85]. This is a common phenomenon in LEDs for virtually all GaInN based QW active regions grown along [0001] direction. The blue-shift is attributed mainly to the screening of the piezoelectric field by free carriers injected into the QW. The magnitude of blueshift varies according to various factors in the LED structures.

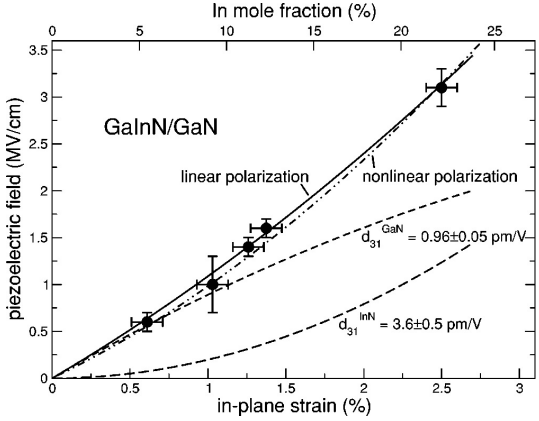

Figure 4.2.: Polarization Field vs In-plane Strain. [68]

According to the Poisson equation, we have the electric field caused by carriers

$$F_{\delta n} = \frac{q\delta n L_Z}{\varepsilon_s}, \tag{4.1}$$

where $F_{\delta n}$ is the electric field caused by free carriers, q is the elementary charge, δn is the three dimensional carrier density, and L_Z is the QW thickness.

4.1.3. Built-in electric field

Assuming an abrupt p-n junction with a donor concentration of N_D and an acceptor concentration of N_A, there is a depletion region due to the diffusion of electrons from n-type side to p-type side and holes from p-type side to n-type side under zero bias. Figure 4.3 shows the typical p-n junction under thermal equilibrium conditions. As a result of the diffusion of electrons and holes, the only charge, which form the space charge as shown in Figure 4.3(a), in the depletion region is from ionized donors and acceptors. The built-in electric field F_{bi} and built-in potential V_{bi} are produced by the space charge at the depletion region, Figure 4.3(b) and (c) show their distribution dependence on position respectively. The direction of the built-in electric field is from n-type side to p-type side and opposite to the direction of polarization field.

From Figure 4.3(b) we can see that F_{bi} reaches a maximum at $x = 0$. According to Poisson's

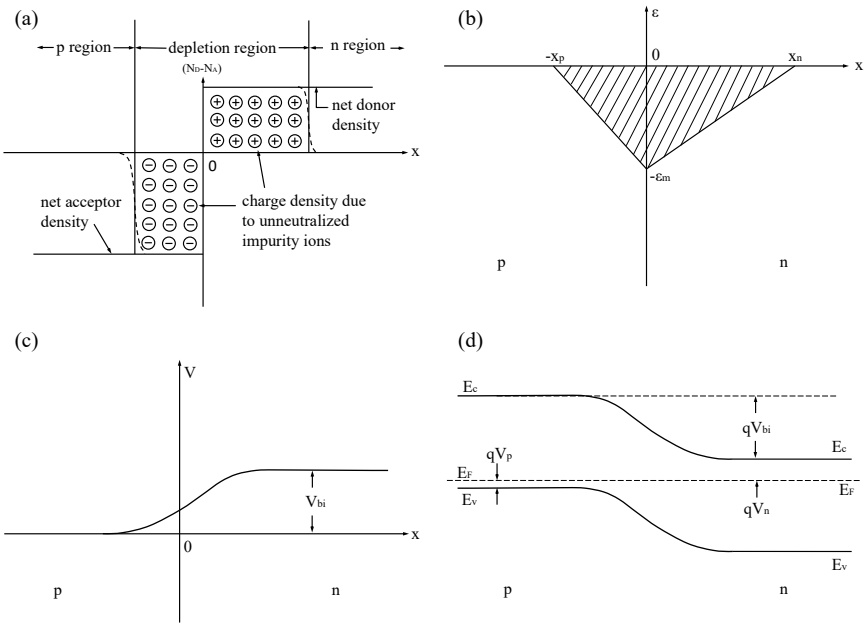

Figure 4.3.: Abrupt p-n junction under thermal equilibrium condition (a) Space charge distribution. (b) Electriv field distribution. (c) Potential variation with distance where V_{bi} is built-in potential. (d) Energy-band diagram [86].

equation we can obtain the electric field shown as the function 4.2 [86]

$$F_{maximum} = F_{x=0} = \frac{qN_D x_n}{\varepsilon_s} = \frac{qN_A x_p}{\varepsilon_s}, \tag{4.2}$$

where q is the elementary charge, x_n and x_p are the depletion region thickness at n-type and p-type respectively. Then the relationship of x_n and x_p can be obtained as the following

$$N_d x_n = N_a x_p. \tag{4.3}$$

According to Figure 4.3(d)

$$qV_{bi} = E_g - (qV_n + qV_p), \tag{4.4}$$

where E_g is the bandgap. Depletion width is given by:

$$W_{p-n} = \sqrt{\frac{2\varepsilon_s}{q}(\frac{N_a + N_d}{N_a N_d})V_{bi}} = x_n + x_p. \tag{4.5}$$

Combining equations 4.3 and 4.5, we can obtain the value of x_n and x_p

$$x_n = \sqrt{\frac{2\varepsilon_s}{q}\frac{N_a}{N_d}(\frac{1}{N_a + N_d})V_{bi}} \tag{4.6a}$$

$$x_p = \sqrt{\frac{2\varepsilon_s}{q}\frac{N_d}{N_a}(\frac{1}{N_a + N_d})V_{bi}}. \tag{4.6b}$$

Then the maximum of built-in electric field will be

$$F_{bi(maximum)} = \frac{qN_D}{\varepsilon_s}\sqrt{\frac{2\varepsilon_s}{q}\frac{N_a}{N_d}(\frac{1}{N_a + N_d})V_{bi}} \tag{4.7a}$$

$$= \frac{qN_A}{\varepsilon_s}\sqrt{\frac{2\varepsilon_s}{q}\frac{N_d}{N_a}(\frac{1}{N_a + N_d})V_{bi}}. \tag{4.7b}$$

Different from the p-n junction, LED with SQW structure insert a well layer (GaInN) and a barrier layer (undoped GaN), between the interface of p-type side and n-type GaN, which can be approximately treated as a p-i-n junction. The intrinsic or un-intentionally doped region is the well and barrier layer, the thickness of intrinsic region, d, will be the sum of thickness of QW and barrier. We can do a similar derivation for the p-i-n junction and obtain the maximum of built-in electric field

$$F_{bi} = \frac{qN_d}{\varepsilon_s} \cdot \frac{\sqrt{d^2 + \frac{2\varepsilon_s}{q}(\frac{1}{N_d} + \frac{1}{N_a}) \cdot V_{bi}} - d}{1 + \frac{N_d}{N_a}}. \tag{4.8}$$

Since the built-in electric field in the whole intrinsic region is constant, which is equal to the maximum of built-in electric field. This means the built-in electric field in the QW is 4.8. Equation 4.8 only shows the built-in electric field under equilibrium condition at zero bias. When forward bias, V_a, is applied on the LED, the built-in potential will reduce to $V_{bi} - V_a$. Besides that, variation of the potential in QW, V_{QW}, caused by the piezoelectric field and screening effect of free carriers within the QW also should be considered.

$$V_{QW} = (F_{carrier} - F_p)L_z, \tag{4.9}$$

Finally the built-in electric field in the QW can be expressed as following

$$F_{bi} = \frac{qN_d}{\varepsilon_s} \cdot \frac{\sqrt{d^2 + \frac{2\varepsilon_s}{q}(\frac{1}{N_d} + \frac{1}{N_a}) \cdot (V_{bi} - V_a + V_{QW})} - d}{1 + \frac{N_d}{N_a}}, \tag{4.10}$$

where F_{bi} is the function of carrier density δn.

4.2. Emission wavelength of LED

The peak emission wavelength of GaN-based QW LED is mainly determined by the bandgap energy of the QW (InGaN). For photoluminescence (PL) conditions, we have

$$E_{PL} = E_g^0 + E_{q,e} + E_{q,h} - e \cdot F_{el} \cdot d_{QW} - E_X, \tag{4.11}$$

where E_g^0 is fundamental strain-free band gap energy of InGaN QW, which is determined by equation 2.1. $E_{q,e}$ and $E_{q,h}$ are the ground-state quantization energy of electron and hole in QW respectively, $e \cdot F_{el} \cdot d_{QW}$ is the effect of QCSE and E_X is the exciton binding energy. Jönen et al. have done some calculation under PL condition [87]. While under electronluminescence (EL) condition, both the screening effect of free carriers and built-in electric field should be considered and they vary with increasing injection current. As shown is the following equation:

$$E_{EL} = E_g^0 + E_{q,e} + E_{q,h} - e \cdot F_{total} \cdot d_{QW} - E_X, \tag{4.12}$$

where, F_{total} should include all the effects of field caused by polarization, free carrier and built-in field of p-n junction,

$$F_{total} = F_{bi} + F_{\delta n} + F_p. \tag{4.13}$$

For high injection conditions, the lower energy states are filled and the emission moves to higher excited states in the QW, which is the so called band filling effect. So besides

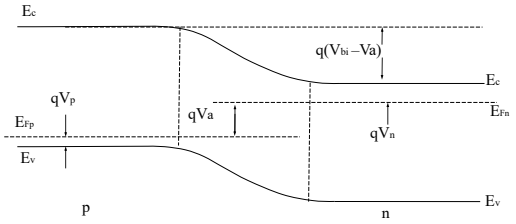

Figure 4.4.: p-n junction under forward bias condition.

the electric field in the QW, the band filling effect can also influence the emission energy but only at very high current density. Considering our experimental conditions that the maximum of current density is about 110A/cm^2, the blue-shift cause by band filling effect is rather small [88]. Then the band filling effect can be neglected for our investigation. We also neglect the variation of the quantization energy, which is justified for these triangular wells (approximation) except for extremely narrow ones.

4.3. Calculation of the carrier density in the QW

From the discussion above, we know that the variation of the peak emission energy is mainly caused by the change of the total electric field in the QW. The piezoelectric field can be obtained from literature [68]. The electric field of free carriers is determined by the Eq 4.1. The built-in electric field under forward bias condition can be determined by the applied forward voltage cross on the p-n junction. However it is difficult to experimentally determine the exact applied forward voltage V_a across on p-n junction because we are not able to estimate the series resistance accurately due to the structure of our LED samples. Here we manage to deduce the relationship between carrier density δn and forward bias V_a according to the quasi Fermi level under quasi thermal equilibrium under EL condition. As shown in Figure 4.4, the applied forward voltage V_a is equal to the separation of Fermi level.

$$N_c = 2\frac{(2\pi m_e^* k_0 T)^{3/2}}{h^3} \tag{4.14a}$$

$$N_v = 2\frac{(2\pi m_h^* k_0 T)^{3/2}}{h^3}, \tag{4.14b}$$

where N_c and N_v are the effective state density for conduction band and valence band respectively. m_e^* and m_h^* are the effective mass of electron and hole respectively, k_0 is Boltzmann

constant, T is temperature, h is Planck constant. For the two dimensional situation in QW

$$N_c = 2\frac{2\pi m_e^* k_0 T}{h^2} \tag{4.15a}$$

$$N_v = 2\frac{2\pi m_h^* k_0 T}{h^2}. \tag{4.15b}$$

Under Boltzmann approximation condition, for the electron and hole we have the relation that:

$$n = N_c exp(-\frac{E_c - E_F^n}{k_0 T}) \tag{4.16a}$$

$$p = N_v exp(\frac{E_v - E_F^p}{k_0 T}), \tag{4.16b}$$

where E_c and E_v are the conduction band and the valence band respectively, E_F^n and E_F^p is the Fermi level for electron and hole respectivley. Under EL condition, injected electrons and holes is equal, $n = p$, then we get:

$$np = N_c N_v exp(\frac{(E_F^n - E_F^p) - (E_c - E_v)}{k_0 T}) = n^2. \tag{4.17}$$

Since the QW locates at the depletion region, the Fermi level of electrons and holes in the QW should be approximately equal to the one in n-type and p-type GaN. Under that precondition wen can make an approximation that the separation of Fermi level in QW is equal to the forward voltage. Based on that approximation we obtain the relationship:

$$V_a = V_{bi} + \frac{k_0 T}{q} ln \frac{n^2}{N_c N_v} \tag{4.18}$$

$$\approx E_{QW} + \frac{k_0 T}{q} ln \frac{n^2}{N_c N_v}, \tag{4.19}$$

where E_{QW} is the bandgap in QW. Here we succeed to correlate the applied forward voltage and carrier density in QW, just as shown equation 4.19.

Using equation 4.12, 4.19 and 4.10, we obtain the dependence of the emission energy on carrier density. A simulation has been done and shows an uncommon 'redshift' and 'minimum' of the emission energy, as shown in Figure 4.5. Actually, this unusual behavior can be explained by the variation of the net field in the QW which is the consequence of the change of both the built-in electric field and the free carriers the electric field. Figure 4.6 is a typical I-V characteristic of our LED. We know that current increase exponentially with increasing applied forward voltage cross on p-n junction. On the one hand, the increasing forward bias will reduce the built-in electric field which has opposite direction with the

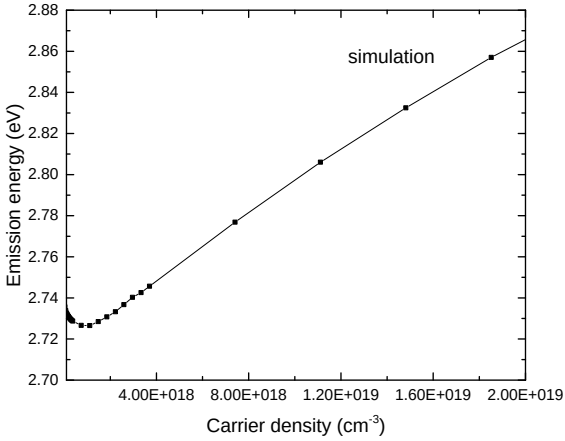

Figure 4.5.: Simulation of emission energy vs carrier density.

piezoelectric field. This means that the increase of the forward voltage causes a redshift of the emission energy. On the other hand, at the very beginning of light emission by the LED, the current is rather small and free carrier density is lower enough to be neglected. This means that the contribution to the total electric field caused by free carriers, which also has the opposite direction to the piezoelectric field, is ignorable. As a result, the decrease of built-in electric field plays a dominant role and the increase of the free carrier field can not compensate it. According to that a redshift is expected under lower current condition with increase forward voltage. As current increases exponentially with increasing forward voltage, injected carrier density increase dramatically while the increase of forward bias become slow. Electic field caused by injected carriers start to have pronounced influence. The effect of injected carriers field exceed the one of forward bias with increasing current and the consequence is that emission energy reach the minimum and begin to increase.

We have measured the emission energy of our LED samples from very low current, as low as about 0.1mA, and the redshift and the minimum were observed just as our theory predicted, as shown in Figure 4.7(a). The minimum of emission energy is 2.7769 eV at 0.91 mA. The redshift phenomenon is quite easy to be overlooked for most common wavelength measurements because it happens at rather low current and is small. The specific current where the emission energy reaches the minimum differs from sample to sample. By comparing the simulation and experimental data we can determine the carrier density for the

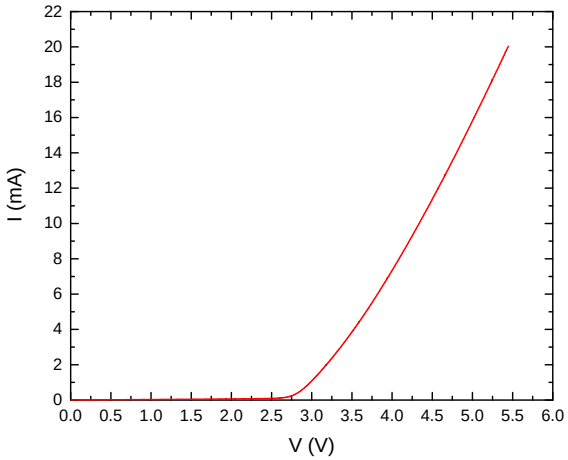

Figure 4.6.: I-V characteristic of SQW blue LED.

corresponding emission energy.

Besides results from our samples, we also observed the 'red-shift' and a 'minimum'of peak emission energy at lower current for a commercial blue LED, as shown in Figure 4.8. Obviously, the peak energy decreases at lower current region and reaches minimum 2.67896eV at about 6.2 mA and then increase with increasing current. The current corresponding to the minimum emission energy is higher than that of our samples. The most likely explanation is that the commercial LED has large contact area which is about 1 mm^2 and five times of our samples. This means that the current density for both commercial LED and our LED is similar. Unfortunately we are not able to do further investigation due to the unknown structure of the commercial LED. Anyway, this finding further confirms that the 'minimum' of emission energy is a common phenomenon which is an important evidence for our theory about the relationship between the emission energy and total electric field.

We calculated the built-in electric field with and without forward bias and the free carriers electric field, as shown in Figure 4.9. The built-in electric field caused by the space charge in p-n junction can reach 0.85 MV/cm without bias, which is smaller than the piezoelectric field (2.25 MV/cm for our case) in the QW but not negligible. Under forward bias conditions, the built-in electric field decreases rapidly and become close to constant. On the other hand, the electric field caused by free carriers increases linearly and becomes greater than the built-in electric field. Apparently, the variation of the electric field of free carriers

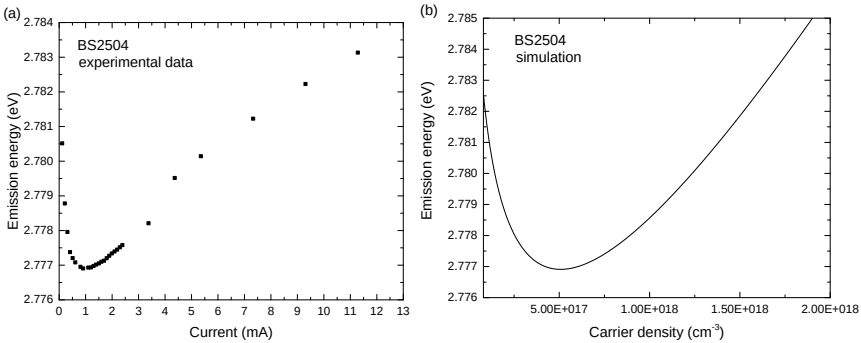

Figure 4.7.: Emission energy dependence on current (a) and simulated emission energy dependence on carrier density(b).

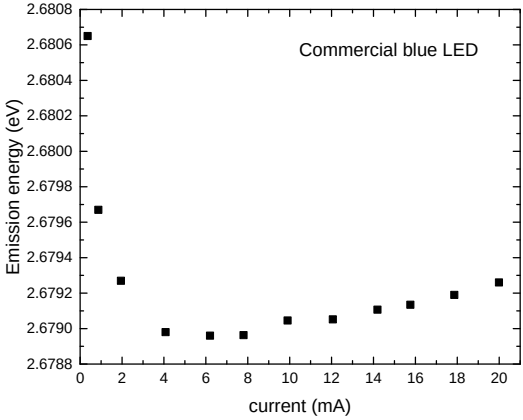

Figure 4.8.: Peak wavelength of commercial blue LED without pack.

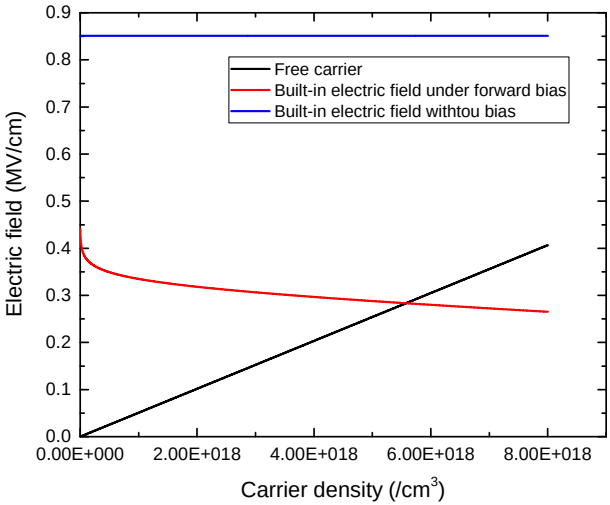

Figure 4.9.: Built-in electric field with and without forward bias, and the free carriers electric field.

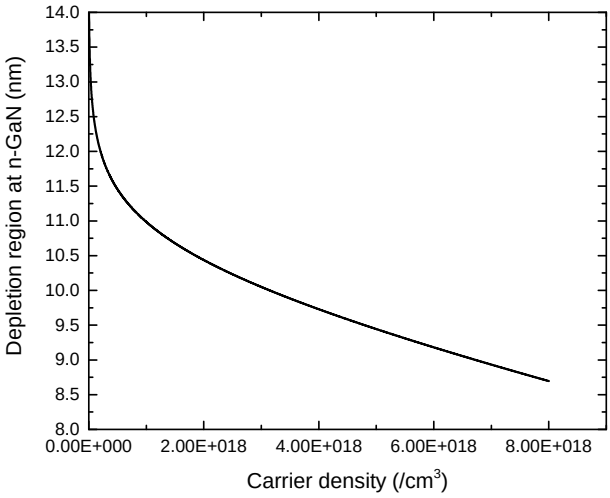

Figure 4.10.: Variation of depletion region at n-GaN side.

is faster than that of the built-in electric field in the interesting rangs of the carrier density. Figure 4.10 shows the variation of depletion region thickness. We can see that it reduces from 13 nm to 9 nm in the interesting carrier density region. According to our calculation, the depletion region thickness is about 27.9 nm under no bias conditions.

4.4. Discussion of the calculated results for the carrier density

During our calculations many parameters from literature or experiment are used, for example doping concentration, thickness of different layers, and effective mass of electron and hole. We need to discuss the effects of these parameters.

4.4.1. Estimation of effective doping level for n-GaN

Unfortunately, the doping profile for the n-type GaN is not exactly known. Between the QW and the normal n-GaN there are two layers of n-GaN which have uncertain Silicon doping. The effective doping level is in the range between $1\times10^{18}/\mathrm{cm}^3$ and $5\times10^{18}/\mathrm{cm}^3$. Here we will do some estimation for the effective doping level.

At low current, namely low carrier density, the IQE is rather low, e.g. IQE is only 10% at 0.3mA, and it drops dramatically towards lower current. This means the recombination processes is dominated by nonradiative recombination. According to the Shockley-Read-Hall recombination, the nonradiative lifetime is independent of carrier density and constant under this condition. First, we can calculate the nonradiative current from the measured current and IQE,

$$I_{nr} = I \cdot (1 - IQE), \tag{4.20}$$

where I_{nr} is the nonradiative current and I is the measured current. Then we can obtain the dependence of peak emission energy on the nonradiative current, as shown in Figure 4.11

We also can deduce the nonradiative current from the calculated carrier density via assuming some certain nonradiative lifetime, which follows the function:

$$I_{nr} = \frac{n_{2D} \cdot e}{\tau_{nr}} \cdot A, \tag{4.21}$$

where n_{2D} is two dimensional carrier density in the QW, e is elementary charge, τ_{nr} is nonradiative lifetime and A is the area of the p-contact for our samples.

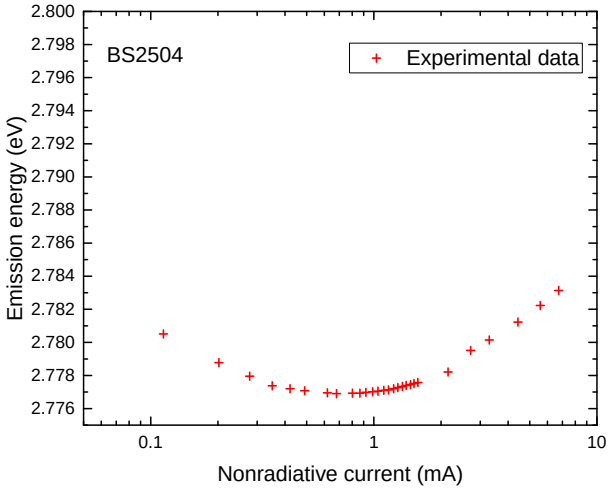

Figure 4.11.: Dependence of emission energy on nonradiative current.

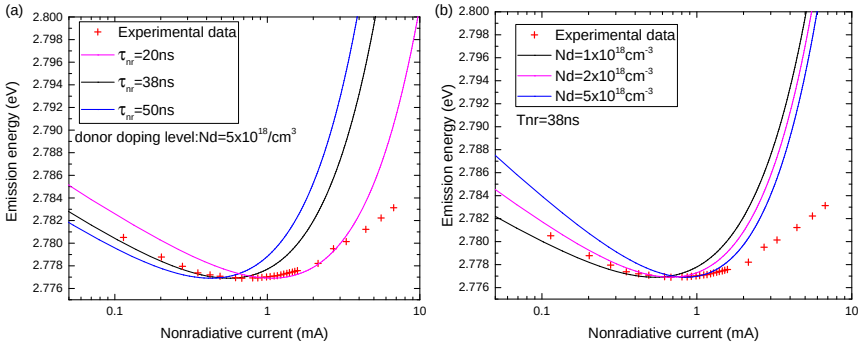

Figure 4.12.: Effects of different nonradiative lifetime (a) and different donor doping level (b) on emission energy.

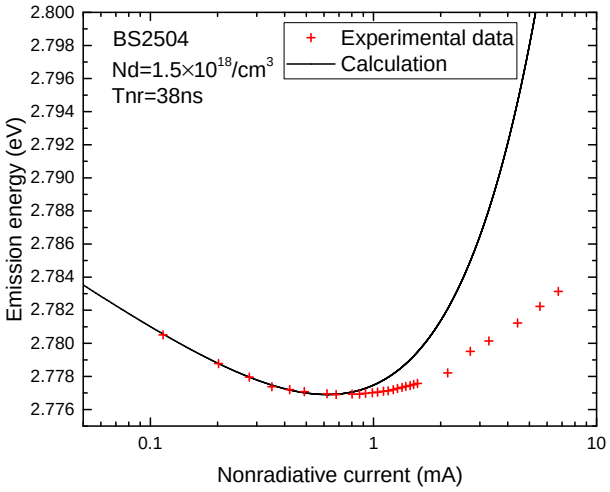

Figure 4.13.: Fitting results with effective donor doping level and nonradiative lifetime.

By adjusting the nonradiative lifetime and the effective doping level, we obtain a good fit for the dependence of emission energy on nonradiative current under low current condition, as shown in Figure 4.13. Here the effective doping level we determined is $1.5\times10^{18}/\text{cm}^3$ and the nonradiative lifetime is 38 ns which is a reasonable value. Of course for different samples the effective doping level might be different. We make a further investigation about the influence of different doping concentration on the lifetime. Regarding the determination of the radiative and nonradiative lifetime we will give detailed discussion in the next chapter. Figure 4.14(a) and (b), show the dependence of the radiative lifetime and the nonradiative lifetime on carrier density for different doping concentration. We can see that a different doping level has no significant influence on the trend of both radiative and nonradiative lifetime.

4.4.2. Effects of intrinsic thickness, effective mass

We calculated the carrier density for different intrinsic thickness, as shown in Figure 4.15. Since the built-in potential is constant for a certain doping, then the built-in electric field in the p-n junction is determined by the thickness of the depletion region. The variation of the thickness of the intrinsic region can affect the emission energy in the QW, as shown in Fig-

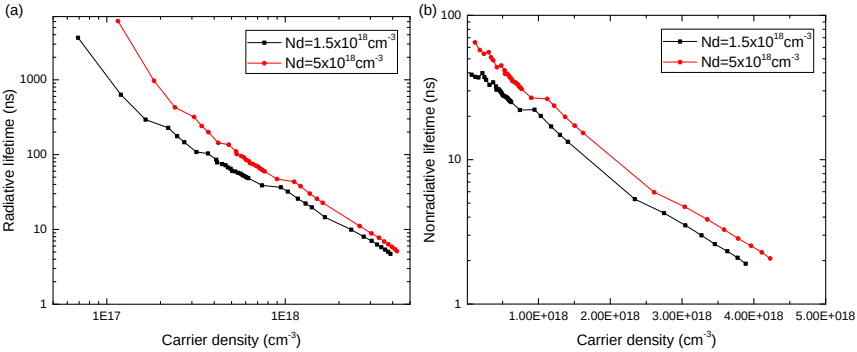

Figure 4.14.: Effects of different doping level on lifetime.

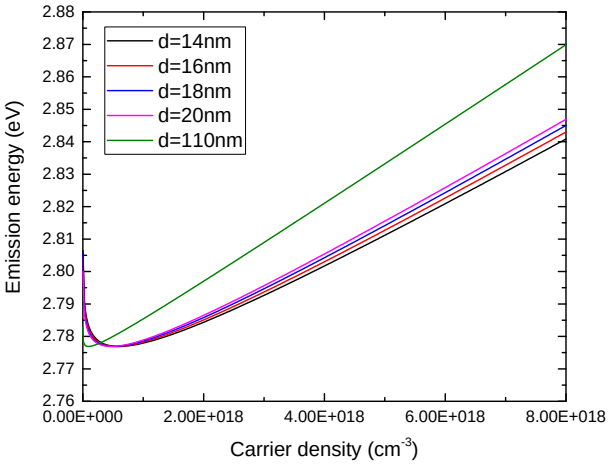

Figure 4.15.: Emission energy for different intrinsic thickness.

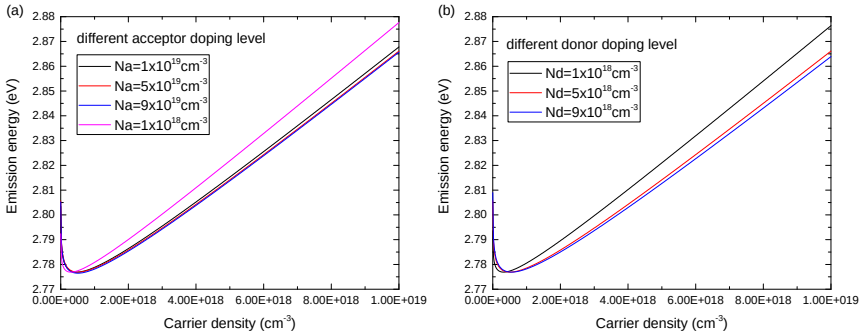

Figure 4.16.: Emission energy for different doping level of acceptor (a) and donor (b).

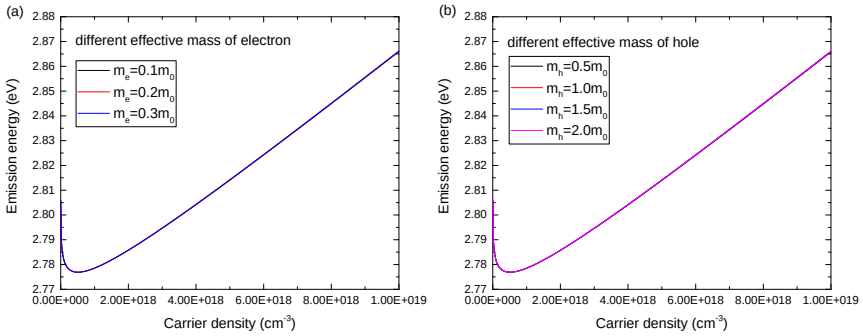

Figure 4.17.: Emission energy for different effective mass of electron (a) and hole (b).

ure 4.15. At the same carrier density, a thicker intrinsic region means a smaller contribution from variation of the applied forward voltage which causes a red-shift. This explains why the curve for thicker intrinsic region has a higher emission energy.

The doping level also influences the built-in electric field, which results in a variation of the emission energy, as shown in Figure 4.16. The mechanism is consistent with the effect of the intrinsic region: lower doping level means smaller built-in electric field, then higher emission energy. But the influence of different doping concentration is small compared to that of the intrinsic region thickness.

The dependence of the emission energy on carrier density for different electron effective mass and hole effective mass also has been calculated, as shown in Figure 4.17. We can see

that in a reasonable range of different effective mass, the difference of emission energy is negligible.

5. Radiative and non-radiative recombination processes in QW

After obtaining the IQE and the determination of the carrier density in the active region, we are able to do a further analysis about the recombination processes in the QW in LEDs. In this chapter, one the one hand we discuss the '*ABC*' model which describe the recombination processes and its limitation. On the other hand, we investigate the recombination mechanism by evaluating the relationship of radiative and non-radiative lifetime dependence on carrier density with considering the effect of the electric field.

5.1. Drawbacks of the ABC model

The efficiency of GaN-based LED is highly dependent on the carrier density within the QW. This has been investigated with different operating current under EL condition [16, 21, 49, 89]. According to the basic recombination processes, as shown in Figure 5.7, the recombination rate R_n can be expressed in a very simple way:

$$R_n = An + Bn^2 + Cn^3, \tag{5.1}$$

where A, B and C is the defect-related, radiative recombination and Auger recombination coefficient respectively, equation 5.1 is well known as the "*ABC*" model . In this model it is assumed that the total recombination rate consists of terms linear, quadratic, and cubic in carrier density, with proportionality factors A, B and C. Since the "*ABC*" model can simply describe the relationship between recombination rate and the carrier density and sounds like quite reasonable, it is the most popular and common model. As a popular tool, "ABC" models are often used to separate the contributions of different recombination mechanisms by their specific dependencies on the charge carrier density n (for example, in references [28, 29, 90, 91, 92, 93]). About this polynomial models, the observed excitation dependency of the emitted light power and quantum efficiencies can indeed adapt quite well.

However, the basic assumptions in these models are rather vague. For example, the same electron and hole ($n = p$) densities and negligible Coulomb interaction between the charge carriers are assumed in the optically active region. Contributions of excitons to the radiative recombination, the screening of polarization fields at high carrier densities and effects due to background carriers thus are completely neglected [94, 95].

Based on the 'ABC' model many explanations are proposed and lots of deduction are developed. One of the models is used to estimate the internal quantum efficiency, as the following equations [74]:

$$\eta_e(p) = \eta_{ext}\,\eta_i, \qquad \eta_i = \frac{Q}{Q + p^{1/2} + p^{-1/2}}, \tag{5.2}$$

$$\eta_e^{max}/\eta_e(p) = \eta_i^{max} + \frac{p^{1/2} + p^{-1/2}}{Q+2}, \tag{5.3}$$

where $\eta_e(p)$ is the current dependent EQE, η_{ext} is the light extraction efficiency (LEE), η_e^{max} is the peak value of EQE, which is determined from the measured light current characteristic. p is normalized optical power $p = P_{out}/P_{max}$, P_{max} is the maximum of optical power, η_i^{max} is the peak IQE value, more detail can be found in the reference [74]. Their results are shown in Figure 5.1. We applied this model to our experimentally determined data and obtained the LEE and the IQE, as shown in Figure 5.2. We can see that the LEE and IQE derived from that model are not consistent with our results. Our LEE has been calibrated with experimental data to make sure the correction of our results. By comparing the fitting results with our other samples, some of the fitted LEE are close to our determination. However, the difference can not be explained. This inconsistence indicates that models based on 'ABC' can not be applied to every situation because it is too simple to describe the recombination processes by the 'ABC' model.

5.2. Determination of the carriers lifetimes in QW

5.2.1. Determination of radiative and non-radiative lifetimes

Since we are able to determine the IQE and the carrier density within the QW, we can derive the radiative and non-radiative lifetime of carriers combining separated 'radiative current'

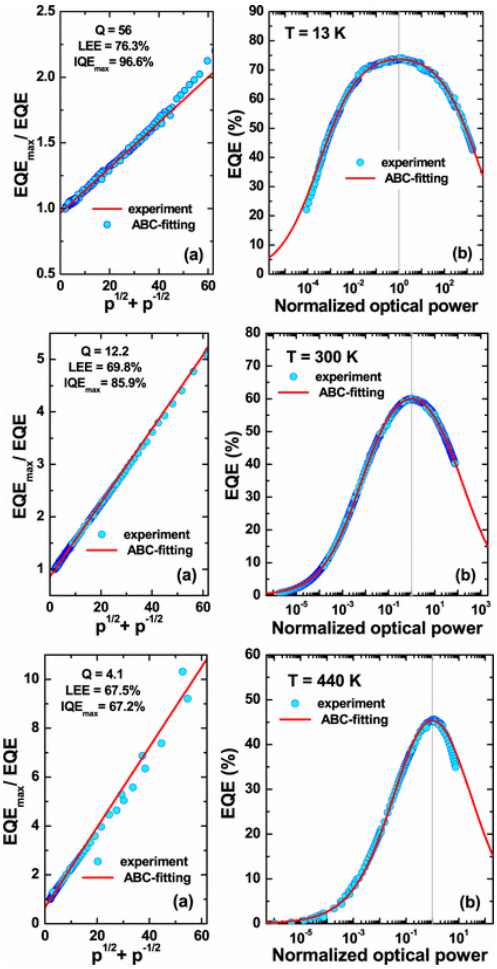

Figure 5.1.: EQE_{max}/EQE ratio as a function of the $p^{1/2} + p^{-1/2}$ combination (a) and experimental and theoretical EQE as a function of the normalized optical power p (b) obtained at various temperatures. Circles indicate experimental points, solid curves are the fittings by ABC-model, using equation 5.2 and 5.3, respectively. Q-factors obtained by fitting and corresponding values of LEE and maximum IQE are given in (a) [74].

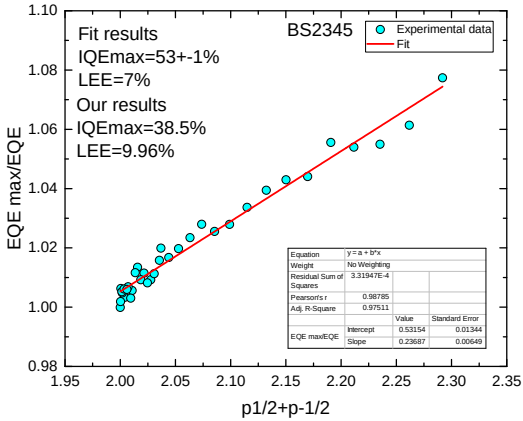

Figure 5.2.: Fit with our experimental data.

and 'non-radiative current' by IQE. According to the definition of current density J, and recombination rate R_n, we have

$$J = \frac{I}{A} = \frac{\delta n V_{QW} e}{A\tau}, \tag{5.4}$$

$$R_n = \frac{dn}{dt} = \frac{\delta n}{\tau}, \tag{5.5}$$

where I is the operating current, A is the area of the p-contact for our sample, δn is the carrier density within the QW, V_{QW} is the volume of the QW, e is the elementary charge, τ is the lifetime of carriers. If the thickness of the QW is L_z, then we will have

$$J = R_n \cdot e \cdot L_z, \tag{5.6}$$

Then the lifetime of free carriers can be derived as following

$$\tau = \frac{\delta n \cdot e \cdot L_z}{J}, \tag{5.7}$$

Since we already have the IQE, which can separate the current density into radiative and non-radiative parts.

$$J_r = J \cdot IQE \tag{5.8a}$$

$$J_{nr} = J \cdot (1 - IQE), \tag{5.8b}$$

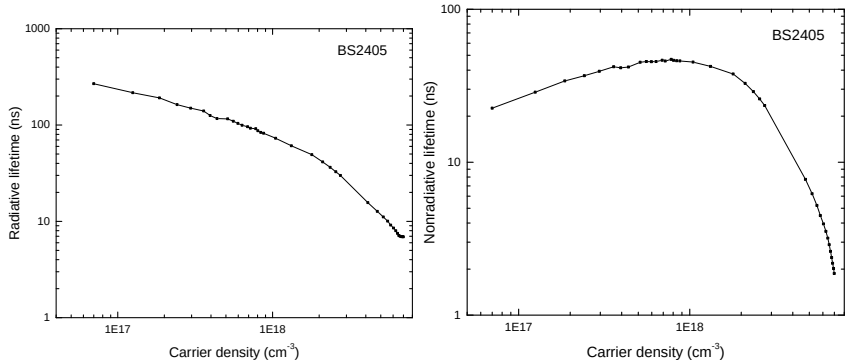

Figure 5.3.: Radiative and non-radiative recombination lifetime vs three dimensional carrier density. Left: radiative lifetime right: non-radiative lifetime.

using equation 5.7 and 5.8, we will have the radiative lifetime τ_r and nonradiative lifetime τ_{nr}:

$$\tau_r = \frac{\delta n \cdot e \cdot L_z}{J \cdot IQE} \tag{5.9a}$$

$$\tau_{nr} = \frac{\delta n \cdot e \cdot L_z}{J \cdot (1 - IQE)}, \tag{5.9b}$$

Figure 5.3 shows the calculated results for the dependence of the lifetime on carrier density, which enable us have a deep investigation of the recombination processes in the QW. Both the radiative lifetime and the nonradiative lifetime are in a reasonable range, and obviously the nonradiative lifetime is shorter than the radiative lifetime. More discussion about the lifetime and carrier density will be carried out in the following sections.

5.2.2. Discussion about the determination of recombination lifetimes

We compare the dependence of radiative lifetime on carrier density of LED sample with that of QW which have comparable structure (similar quantum well thickness and indium composition) with the QW of LED sample. The determination of the lifetime and the carrier density and more detail for the QW sample can be found in reference [95]. As shown in Figure 5.4, at lower carrier density region (about $10^{17}/\mathrm{cm}^3$), both two samples have similar radiative lifetime. While with increase of the carrier density, the dependence of

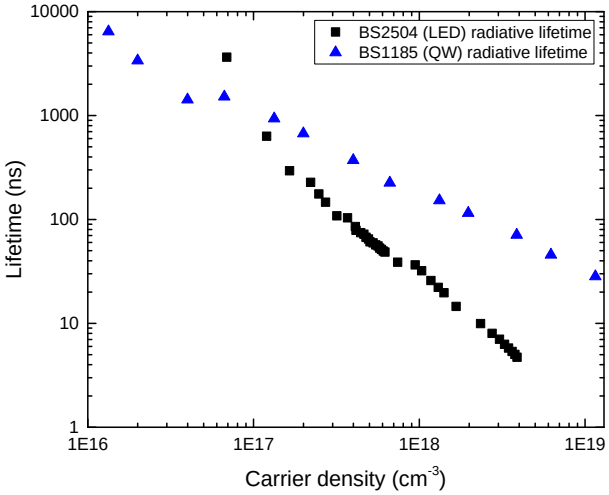

Figure 5.4.: Comparison of radiative lifetime for LED and QW.

radiative lifetime on carrier density of LED sample has steeper slope than that of QW. This behavior can be explained if we examine the two different ways of determination of the carrier density for the two samples. On the one hand, the carrier density for the QW is determined by counting the number of photon injected into the active region, which means the carrier density is the total carrier density including excitons and free carriers. On the other hand, the carrier density for the LED is obtained by relating the carrier density, blue-shift of emission energy and variation of total electric field in the QW in LED. Regarding the fact that only free carriers contribute to the total electric field, which means the carrier density is actually the free carrier density. In other words, the 'carrier density' in Figure 5.4 is total carrier density (free carrier plus excitons) and free carrier density for QW and LED respectively. This can explain that at low carrier density region both two samples have similar radiative lifetime, because the total carriers are dominated by free carriers. Exciton population fraction increase with increasing total carrier density, which is consistent with the calculation in Figure 5.5 [96].

The equilibrium between excitons and free carriers can be approximated by a law of mass action (Saha equation),

$$\frac{np}{x} = C(T), \tag{5.10}$$

where n, p and x are the free electron, hole and exciton densities, respectively. $C(T)$ is

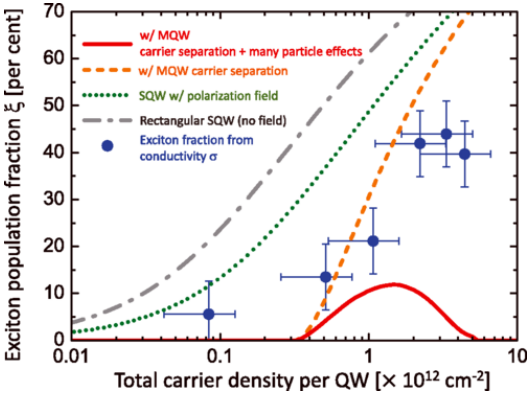

Figure 5.5.: Dependence of exciton population fraction on total carrier density. The green dotted line is for a single polarized QW [96].

equilibrium constant and depends on temperature [96]. Using the method in reference [96], we obtain the relationship of free carrier density and total carrier density, as shown in Figure 5.6.

5.3. Radiative recombination

5.3.1. Classic radiative recombination mechanism and theory

There are two types of free carriers, electrons and holes, in doped or undoped semiconductor. Under equilibrium conditions without external stimulation, the product of the electron and hole concentrations is, at a given temperature, a constant [97],

$$n_0 p_0 = n_i^2, \tag{5.11}$$

where n_0 and p_0 are the equilibrium electron and hole concentrations and n_i is the intrinsic carrier concentration. There are three different ways by which excess carriers can be created: (i) absorption of light, (ii) injection by current, (iii) bombardment by energetic particles [98]. The total carrier density is then given by the sum of equilibrium and excess carrier density

$$n = n_0 + \delta n \tag{5.12a}$$

$$\text{and } p = p_0 + \delta p, \tag{5.12b}$$

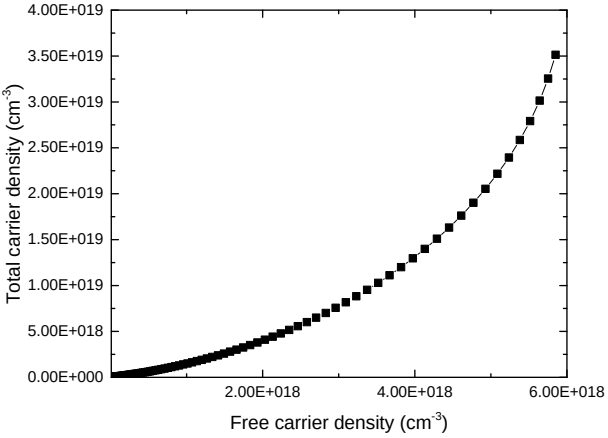

Figure 5.6.: Relationship of total carrier density and free carrier density.

where δn and δp are the excess electron and hole concentrations, respectively.

For electrons and holes excited to a non-equilibrium state, basically there are three channels for their recombination: (a) recombine via recombination centers produced by defects, (b) radiative recombination by emitting photons and (c) recombine with transferring the energy to free electrons or holes (which is referred as Auger recombination), as shown in Figure 5.7.

Now we discuss the radiative recombination process. In equilibrium, the generation rate equals the recombination rate, which itself is proportional to the product of $n_0 p_0$,

$$G = R_{sp}^0 = B_r n_0 p_0, \tag{5.13}$$

where R_{sp}^0 is spontaneous recombination rate, B_r is a proportionality constant. The recombination rate obeys the equation:

$$R = B_r np = B_r (n + n_0)(p + p_0). \tag{5.14}$$

When excess carriers decay, the instantaneous electron density follows the differential equation:

$$\frac{dn}{dt} = G - R = B_r (n_0 p_0 - np). \tag{5.15}$$

According to equation 5.12 and δn=δp, then we obtain:

$$\frac{d(\delta n)}{dt} = -B_r (n_0 + p_0 + \delta n)\delta n. \tag{5.16}$$

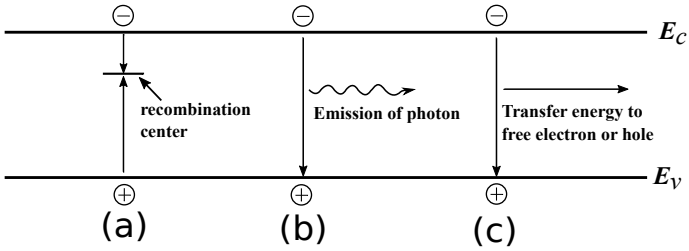

Figure 5.7.: Illustration of recombination precesses (a) defect-related recombination (b) radiative recombination (c) Auger recombination.

Solve equation 5.16, we obtain an exponential time dependence for the decay of the excess carriers:

$$\delta n(t) = \delta n(0) e^{-t/\tau_r}, \tag{5.17}$$

where $\delta n(0)$ is the initial excess electron concentration, τ_r is the lifetime of excess electron, which is given by:

$$\tau_r = \frac{1}{B_r(n_0 + p_0 + \delta n)}. \tag{5.18}$$

Under the condition of low injection satisfying $\delta n \ll (n_0 + p_0)$, the lifetime is given by:

$$\tau = \frac{1}{B_r(n_0 + p_0)}, \tag{5.19}$$

On the other hand, for high levels of injection, $\delta n \gg (n_0 + p_0)$, and thus

$$\tau = \frac{1}{B_r \delta n}. \tag{5.20}$$

Wurtzite GaN has a direct band gap. This means both the minimum of the conduction band and the maximum of the valence band are located at the Γ-point, thus in the center of the Brillouin zone [99, 100, 101]. In a non-degenerate semiconductor (i.e. occupation in the bands can be described by a Boltzmann distribution), a semi-classical approach can be used to microscopically describe the radiative recombination processes, the spontaneous emission rate R_{sp} for the bulk semiconductors is given by [98]

$$R_{\mathrm{sp}} = \underbrace{\frac{e^2 N h \nu_{\max}}{2\pi\varepsilon_0 \hbar^2 m_0^2 c^3} \left(\frac{2\pi\hbar^2}{k_{\mathrm{B}} T}\right)^{3/2} \left(\frac{1}{m_{\mathrm{e}} + m_{\mathrm{h}}}\right)^{3/2} \left\langle |p_{\mathrm{LB}\to\mathrm{VB}}|^2 \right\rangle}_{=:B_r} \cdot n \cdot p, \tag{5.21}$$

where, N is the refractive index of the semiconductor, T is the temperature, $h\nu_{max}$ the peak energy of spectrum for the emitted light, m_e and m_h is the effective mass of electron in the conduction band and hole in the valence band. n and p are the carrier densities of the electrons and the holes. $\left\langle |p_{\mathrm{LB}\to\mathrm{VB}}|^2 \right\rangle$ is the square of absolute momentum matrix element for the transition from the conduction band to the valence band. From the equation we can see that the term B_r is the radiative recombination coefficient.

5.3.2. Effects of internal electric field on recombination probability

Regarding the facts that the total electric field in the QW can change the oscillator strength and the total carrier density is consist of free carriers and excitons, both of the two factors should be considered when we investigate the dependence of radiative lifetime on carrier density. As shown in Figure 5.8, we observed a quite linear dependence of the radiative lifetime on the carrier density at relative lower carrier density region when we plot them in a double log way and the slope is about -0.286±0.005. This result can not be explained with the simple relationship of radiative part (Bn^2) in the '*ABC*' model because the slope should be -1 according to $\tau_r = 1/Bn$, B is constant. Here, actually, B should not be constant but proportional to the radiative recombination probability, which exponentially depends on net electric field in the QW according to our calculation [102], as shown Figure 5.9. As we discussed earlier, the net electric field increases first then reaches a maximum and then decreases during increasing the forward voltage under EL conditions. The range of variation of net electric field for sample BS2405 is from 1.70 MV/cm to 1.56 MV/cm. From Figure 5.9 we can see that the recombination probability varies from about 0.1 to 0.15 caused by the decreasing of net electric field from about 1.70MV/cm to 1.5MV/cm. We can conclude that the net electric field definitely contributes to the decrease of the radiative lifetime considering that the slope is not -1. At higher carrier density region, radiative lifetime is nearly constant. It is easier to understand if we examine the exciton population fraction at higher carrier density (higher than $1\times10^{19}/\mathrm{cm}^3$), which is beyond 65% at $1\times10^{19}/\mathrm{cm}^3$, as shown in Figure 5.10 [96].

The same analysis was performed on variation sample with the same nominal structure. The similar behavior was observed, as shown in Figure 5.11, the slope of the sample is approximately -0.83 ± 0.03, which can not be explained with the simple Bn^2, radiative recombination part in the '*ABC*' model.

We growed a series of samples with nominally same structure and do the same analysis. These sample can be attribute to two groups: BS24 series and BS25 series. The different

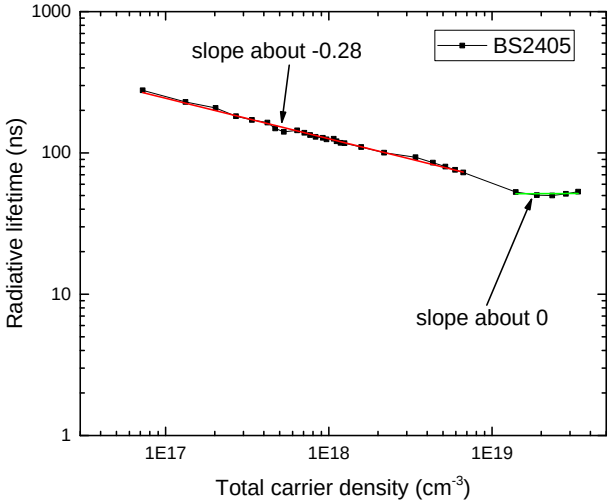

Figure 5.8.: Radiative lifetime dependence on carrier density (a) and net electric field in QW (b).

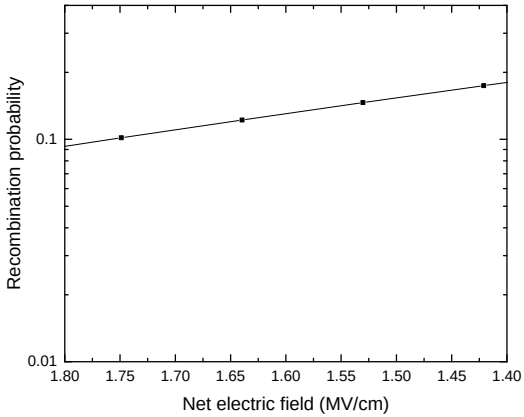

Figure 5.9.: Recombination probability dependence on electric field.

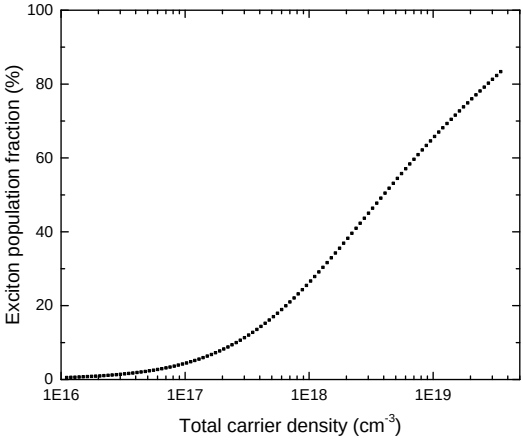

Figure 5.10.: Dependence of exciton population fraction on the total carrier density [96].

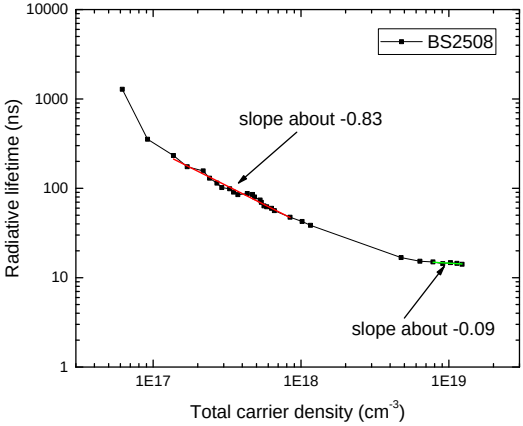

Figure 5.11.: Linear fit of radiative lifetime vs carrier density.

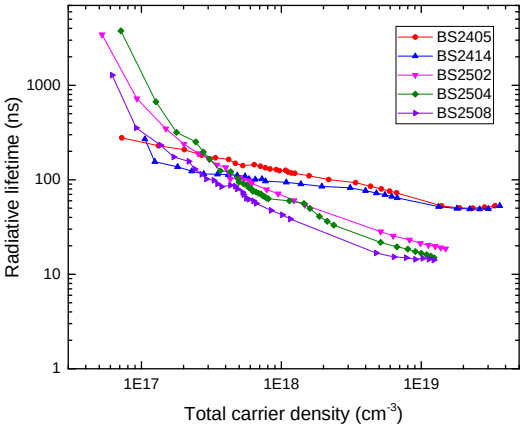

Figure 5.12.: Radiative lifetimes for different samples.

emission energy for the two groups samples might be caused by a the fluctuation of the QW thickness, a typical thickness fluctuation around 0.3 nm, i.e. 1 monolayer has been verified [103]. BS25 series have thinner QW than BS24 series. This will mean the separation of electron and hole wavefunction in active region is larger for BS24 series than that of BS25. As a result, the radiative lifetime for the BS24 series should be longer than that of BS25 series, which is consistent with the calculated results.

5.4. Non-radiative recombination

5.4.1. Theory on nonradiative recombination mechanism

One of the most common cause for non-radiative recombination events are defects in the semiconductor. This effects include unwanted foreign atoms, native defects and dislocations. All such defects have energy level structure that are different from substantial semiconductor atoms. And it is quite common for such defects to form energy levels within the forbidden gap of the semiconductor. Energy levels within the forbidden gap of the semiconductors are efficient recombination centers, in particular if the energy level is close to the middle of the gap. The recombination of electrons and holes via deep levels caused by defects, as shown in Figure 5.7 process(a), was first analyzed by Shockley, Read [104] and

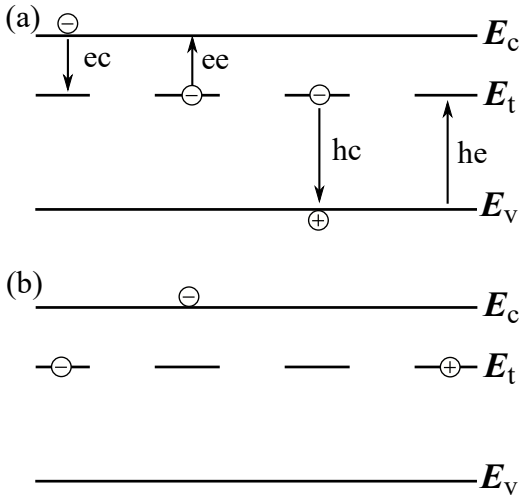

Figure 5.13.: Nonradiative recombination prosesses before(a) and after(b).

Hall [105]. The Shockley-Read-Hall (SRH) recombination can be described by four processes: electron capture (ec), electron emission (ee), hole capture (hc), and hole emission, as shown in Figure 5.13. If we define that: R_{ec}, R_{ee}, R_{hc}, and R_{he} is the electron capture probability, electron emission probability, hole capture probability, and hole emission probability per unit time per unit volume respectively. In general, the rate of electron capture probabilty is a function of electron density, capture cross section and density of the empty traps. The rate of electron emission probability depends only on the electron emission rate and the density of traps being filled by the electrons. For the holes the situation is similar. Thus, we have

$$R_{ec} = c_e \cdot n \cdot N_t(1 - f_t) \tag{5.22a}$$

$$R_{ee} = e_e \cdot N_t \cdot f_t \tag{5.22b}$$

$$R_{hc} = c_h \cdot p \cdot N_t f_t \tag{5.22c}$$

$$R_{he} = e_h \cdot N_t \cdot (1 - f_t), \tag{5.22d}$$

where c_e and c_h are the electron and hole capture coefficients. e_e and e_h are the electron and hole emission rates. N_t is the trap density. f_t is the distribution function of a carrier at

the trap state, is given by

$$f_t = \frac{1}{1+exp(\frac{E_t-E_f}{K_BT})}. \tag{5.23}$$

The non-radiative recombination rate through a deep level with trap energy E_t and concentration N_t is given by

$$R_{sp} = \frac{p_0\delta n + n_0\delta p + \delta n\delta p}{(N_t\nu_p\sigma_p)^{-1}(n_0+n_1+\delta n)+(N_t\nu_n\sigma_n)^{-1}(p_0+p_1+\delta p)}, \tag{5.24}$$

where $\delta n = \delta p$, ν_n and ν_p are the electron and hole thermal velocities, and σ_n and σ_p are the capture cross sections of the traps. The quantities n_1 and p_1 are the electron and hole concentrations if the Fermi energy is located at the trap level, which are given by

$$n_1 = n_i \cdot exp(\frac{E_t - E_{Fi}}{kT}) \tag{5.25a}$$

$$p_1 = n_i \cdot exp(\frac{E_{Fi} - E_t}{kT}). \tag{5.25b}$$

Auger recombination is another important non-radiative recombination processes. These processes involve three particles and are shown schematically in Figure 5.7 process(c). Basically there are two kinds of Auger processes: electron-electron-hole ("eeh") process which is more likely to happen in n-type semiconductors due to the abundance of electrons, and hole-hole-electron-hole processes ("ehh") which is more likely to happen in p-type semiconductors due to the abundance of holes.

$$R_{Auger,eeh} = C_{eeh}n^2p \tag{5.26a}$$

$$R_{Auger,hhe} = C_{hhe}np^2, \tag{5.26b}$$

where C_{eeh} and C_{hhe} are Auger coefficients.

Auger recombination reduces the luminescence efficiency of semiconductor emitting devices only at very high excitation intensity or at very high injection currents. This is due to the cubic carrier concentration dependence. At lower carrier concentrations, the Auger recombination rate is very small and can be neglected for practical purposes. Under high injection condition that the non-equilibrium carriers have a higher concentration than equilibrium carriers, the Auger rate equations can be written to

$$R_{Auger} = Cn^3, \tag{5.27}$$

Where C is called Auger coefficient, which can be determined by calculation and experiments, for example, Hader et al. computed Auger coefficient C of 3.5×10^{-34} cm^6/s [23], experimentally measured Auger recombination coefficient of $1.8\pm0.2\times10^{-31}cm^6/s$ by M. Brendel et al. [40].

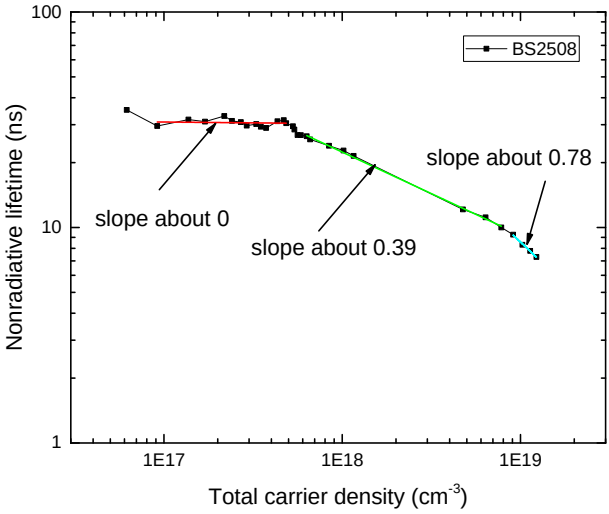

Figure 5.14.: Dependence of nonradiative lifetime on carrier density.

5.4.2. Nonradiative recombination in SQW LED

The method determining the nonradiative lifetime in section 5.2 enable us make an investigation about the dependence of nonradiative lifetime on carrier density.

Figure 5.14 shows the nonradiative lifetime of BS2508 vs carrier density. The nonradiative lifetime is constant at lower carrier density region, as noted by red line, which is the typical SRH recombination. It starts to decrease with increasing carrier density. It can be seen that the nonradiative lifetimes at high carrier densities drops sharply. The slope is getting larger and reaches about 0.78, close to 1. This behavior can be explained by an increasing fraction of contribution of Auger recombination when the carrier density becomes higher. All the observations indicate that the nonradiative lifetime in the classical picture come from two contributions: a constant part due to defect-related recombination and a $1/n^2$ contribution due to Auger recombination.

As shown in Figure 5.15, the nonradiative lifetime is not constant but increase at low carrier density region. This is in contrast to the common assumption of density independent Shockley-Read-Hall (SRH) coefficients A=$\tau_{nr,SRH}^{-1}$ in simple ABC models. It is still a strange behavior since there should be no background carriers in the QW which locate

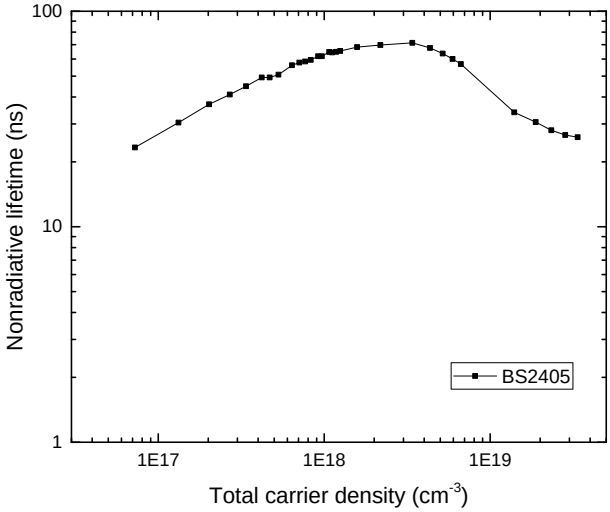

Figure 5.15.: Abnormal nonradiative recombination behavior.

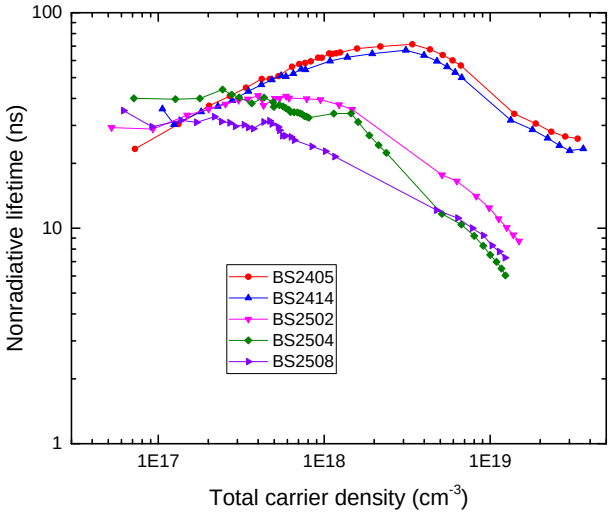

Figure 5.16.: Comparison of two behaviors: normal and abnormal dependence of nonradiative lifetime on carrier density.

at the depletion region. At higher carrier density region, the slope increase with increasing carrier density and the slope decrease at very high carrier density. Actually, all BS24 series samples show the abnormal phenomenon but BS25 series shows what we expect, as shown in Figure 5.16. This is still a mystery and need to be further investigated. Still, all the samples have quite similar nonradiative lifetime at low carrier density.

6. Conclusions and future works

6.1. Conclusions of this thesis

- **Calculation of extraction efficiency and calibration with experimental results**

  For the calculation of the extraction efficiency, most methods are based on the models of the LED structures in the software used for optical simulation. To measure the extraction efficiency directly through experiments is quite challenging even though some direct measurements have been proposed [106, 107]. A reliable and accurate evaluation of the extraction efficiency is still very necessary to determine the IQE and further analyze the LED. Based on the structure of our LED samples, we have managed to develop an approach to calculate the extraction efficiency. During the calculation, the complex dielectric functions of GaN, sapphire, and Pt, the dispersion of the dielectric functions, and TE polarization of the emission are taken into account. Due to the nature of the high refractive index of GaN, the escape angle for light is small which results in a rather low extraction efficiency. Some assumptions are also made, e.g. ideal flat interfaces among different layers and ideal metallic mirror of the p-contact. Different samples with nominally identical structure except for a variation of cap thickness, which should have quite similar internal quantum efficiency but different external quantum efficiency, are grown to calibrate our calculation. By adjusting the reflectivity and phased shift a quite good fit with the experimental data has been achieved. The calibration processes eliminates the difference between the calculated and real extraction efficiency and enables us obtain a reliable way to determine the internal quantum efficiency.

- **Determination of carrier density in the SQW of a LED**

  By analyzing the effect of electric field within QW on the emission energy of a LED, we established the correlation of emission energy, carrier density, and variation of electric field. We find that the built-in electric field of p-n junction caused by space

charge have a significant influence on the total electric field in the QW. The built-in electric field has the opposite sign of the piezoelectric field and decreases with increasing applied forward voltage. At the same time the free carrier electric field increases associated with the rising operating current. As a consequence of the variation of both factors, there exist a minimum of the emission energy, where the influence of free carriers exceeds that of the built-in electric field. We indeed observed the minimum at relative low current, which allow us to experimentally calibrate our calculation for different LED samples.

- **Analysis of recombination processes for SQW blue LED**

  After determination of the carrier density and a reliable IQE, we are able to calculate the radiative lifetime and nonradiative lifetime and investigate their dependence on carrier density. The typical Shockley-Read-Hall recombination has been observed. Auger recombination starts to play a role with increasing carrier density. Some samples show abnormal increase of nonradiative lifetime at low current density region and the reason is still unclear. A possible reason might be the deviation of parameters of the LED structure, which need to be further checked and investigated.

6.2. Future work

- **Injection efficiency under EL condition**

  We have found an optical approach the measure the injection efficiency for the LED under electroluminescence condition [50]. At low current injection we have an good estimation about the injection efficiency (approximately 80%). However, a strange behavior that injection efficiency is negative was observed under high current operation. We still can not explain that. When we apply this method on an unpacked commercial blue LED and we obtained the injection efficiency which is as high as 83% and is constant. On the one hand we need examine and improve our experimental set for the measurement. On the other hand, optimization for our LED structure needs to be done, e.g. performing standard processes for the contact.

- **Further investigation of radiative and nonradiative recombination**

  Our works focus on the determination of extraction efficiency and carrier density. We studied the radiative and nonradiative lifetime dependence on carrier density for

only few typical c-plane LED samples. While the final purpose is the to better understand the recombination processes in QW in LED and even solve the efficiency droop problem. In order to do that, more detail about the radiative and nonradiative recombination processes need to be investigated, therefore more well designed LED structures are required. For instance, LEDs intend to analyze the influence of electric field and design of structure which could be used to investigate SRH recombination and Auger recombination. Additionally, we need try to expand our investigation to semi-polar or non-polar structure LED because.

A. Calculation of extraction efficiency

In this appendix, we will show the detailed processes of the calculation of the extraction efficiency. For the two light rays E_1 and E_2 (blue lines) as shown in Figure A.1, when they propagate through the interfaces of GaN and sapphire, sapphire and air, GaN and metallic mirror (Platinum contact), they follow Snell-Descartes law, Eq Eq 3.7, and the Fresnel formulae, Eq 3.9. For a specific light ray with incident angle θ , we have

$$\frac{\sin\theta_0}{\sin\theta_1} = \frac{n_{sapphire}}{n_{GaN}} \tag{A.1}$$

$$\frac{\sin\theta_1}{\sin\theta_2} = \frac{n_{air}}{n_{sapphire}} \tag{A.2}$$

where n_{GaN}, $n_{sapphire}$, and n_{air} are the refractive index of GaN, sapphire and air, respectively. Then we can determine θ_1 and θ_2. For light ray E_1, from GaN to sapphire, and from sapphire to air, the amplitude of the transmitted light follow the equations,

$$A_{\parallel,sapphire} = \frac{2n_{GaN}\cos\theta_0}{n_{sapphire}\cos\theta_0 + n_{GaN}\cos\theta_1} A_{\parallel,GaN} \tag{A.3a}$$

$$A_{\parallel,air} = \frac{2n_{sapphire}\cos\theta_1}{n_{air}\cos\theta_1 + n_{sapphire}\cos\theta_2} A_{\parallel,sapphire} \tag{A.3b}$$

A is the amplitude of the electric vector of incident light, $A_{\parallel,out} = f(\theta)A_{\parallel}$. For the light ray E_2, in ideal case, it follows the same equation. The only difference from E_1 is the phase shift when it is reflected by the metallic mirror

Intensity of light I is proportional to the square of its amplitude

$$I \propto A^2 \tag{A.4}$$

$$\tag{A.5}$$

Then we have

$$I_{1,out} = f(\theta)\cdot A^2 \tag{A.6a}$$

$$I_{2r,out} = f(\theta)\cdot r\cdot A^2 \tag{A.6b}$$

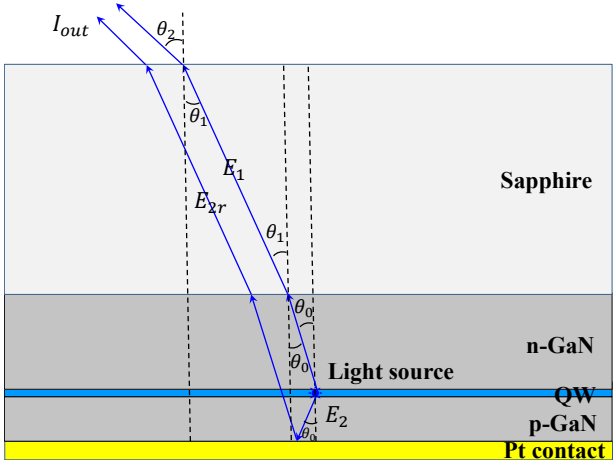

Figure A.1.: Light path in the sample

where r is practical reflection coefficient due to the roughness of the interface of GaN and metallic mirror. E_1 and E_2 are coherent, for the total light intensity I_{out}

$$I_{out} = I_{1,out} + I_{2r,out} + 2\sqrt{I_{1,out} I_{2r,out}} \cos\delta \tag{A.7}$$

δ is phase shift, which is determined by two contributions:

$$\delta = \delta_{\Delta L} + \delta_r \tag{A.8}$$

where $\delta_{\Delta L}$ is the phase shift due to the optical path length differences, and δ_r is the phase shift upon reflection off the metallic mirror, namely phase shift between E_{2r} and E_2, which is a fitting parameter.

$$\Delta L = \frac{d}{\cos\theta}(1 + \cos 2\theta) \tag{A.9}$$

where ΔL is the path difference, d is the cap thicknessas shown in Figure A.2. The corresponding phase difference $\delta_{\Delta L}$ is

$$\delta_{\Delta L} = \frac{2\pi}{\lambda}\Delta L \tag{A.10}$$

where λ is the peak wavelength. The extraction efficiency is

$$\eta_{EXE} = \frac{\int_0^{\theta_{critical}} I_{out} d\theta}{\int_0^{2\pi} I_o d\theta} \tag{A.11}$$

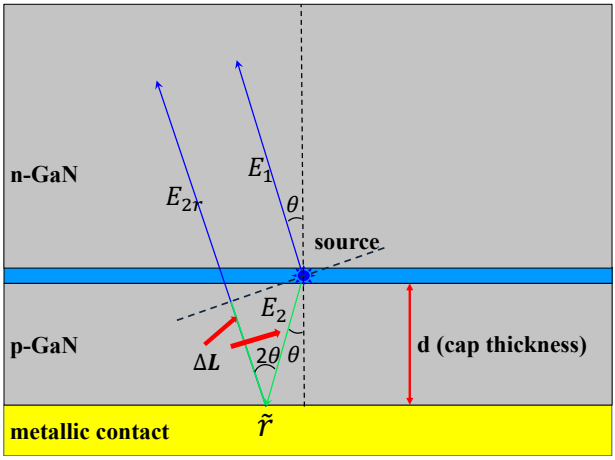

Figure A.2.: Light path at the interface of metal-sapphire in the sample

where $\theta_{critical}$ is determined by the equation

$$\theta_{critial} = \arcsin\left(\frac{n_{air}}{n_{sapphire}} \sin\theta_2\right) = \arcsin\frac{n_{air}}{n_{sapphire}} \tag{A.12}$$

Bibliography

[1] S. Nakamura, *Nobel Lecture: Background story of the invention of efficient blue InGaN light emitting diodes**, Rev. Mod. Phys. **87**, 1139 (2015).

[2] H. J. Round, *A note on carborundum*, Electrical world **49**, 309 (1907).

[3] H. Maruska, D. Stevenson, and J. Pankove, *Violet luminescence of Mg-doped GaN*, Applied Physics Letters **22**, 303 (1973).

[4] J. Pankove, E. Miller, D. Richman, and J. Berkeyheiser, *Electroluminescence in GaN*, Journal of Luminescence **4**, 63 (1971).

[5] H. Amano, M. Kito, K. Hiramatsu, and I. Akasaki, *P-Type Conduction in Mg-Doped GaN Treated with Low-Energy Electron Beam Irradiation (LEEBI)*, Japanese Journal of Applied Physics **28**, L2112 (1989).

[6] S. Nakamura, T. Mukai, M. Senoh, and N. Iwasa, *Thermal Annealing Effects on P-Type Mg-Doped GaN Films*, Japanese Journal of Applied Physics **31**, L139 (1992).

[7] S. Nakamura, N. Iwasa, M. Senoh, and T. Mukai, *Hole Compensation Mechanism of P-Type GaN Films*, Japanese Journal of Applied Physics **31**, 1258 (1992).

[8] S. Nakamura, M. Senoh, and T. Mukai, *P-GaN/N-InGaN/N-GaN Double-Heterostructure Blue-Light-Emitting Diodes*, Japanese Journal of Applied Physics **32**, L8 (1993).

[9] S. Nakamura, T. Mukai, and M. Senoh, *Candera-class high-brightness InGaN/AlgaN double-heterostructure blue-light-emitting diodes*, Applied Physics Letters **64**, 1687 (1994).

[10] S. Nakamura, M. Senoh, N. Iwasa, S. ichi Nagahama, T. Yamada, and T. Mukai, *Superbright Green InGaN Single-Quantum-Well-Structure Light-Emitting Diodes*, Japanese Journal of Applied Physics **34**, L1332 (1995).

[11] S. Nakamura, M. Senoh, N. Iwasa, and S.-i. Nagahama, *High-brightness in InGaN blue, green and yellow light-emitting diodes with quantum well structures*, Jpn. J. Appl. Phys. **34**, L797 (1995).

[12] Y. Narukawa, M. Ichikawa, D. Sanga, M. Sano, and T. Mukai, *White light emitting diodes with super-high luminous efficacy*, Journal of Physics D: Applied Physics **43**, 354002 (2010).

[13] S. Saito, R. Hashimoto, J. Hwang, and S. Nunoue, *InGaN Light-Emitting Diodes on c -Face Sapphire Substrates in Green Gap Spectral Range*, Applied Physics Express **6**, 111004 (2013).

[14] T. Langer, A. Kruse, F. A. Ketzer, A. Schwiegel, L. Hoffmann, H. J?nen, H. Bremers, U. Rossow, and A. Hangleiter, *Origin of the "green gap": Increasing nonradiative recombination in indium-rich GaInN/GaN quantum well structures*, physica status solidi (c) **8**, 2170 (2011).

[15] G. Verzellesi, D. Saguatti, M. Meneghini, F. Bertazzi, M. Goano, G. Meneghesso, and E. Zanoni, *Efficiency droop in InGaN/GaN blue light-emitting diodes: Physical mechanisms and remedies*, Journal of Applied Physics **114**, (2013).

[16] T. Mukai, M. Yamada, and S. Nakamura, *Characteristics of InGaN-Based UV/Blue/Green/Amber/Red Light-Emitting Diodes*, Jpn. J. Appl. Phys. **38**, 3976 (1999).

[17] Y. Yang, X. A. Cao, and C. Yan, *Investigation of the Nonthermal Mechanism of Efficiency Rolloff in InGaN Light-Emitting Diodes*, IEEE Transactions on Electron Devices **55**, 1771 (2008).

[18] W. Sun, M. Shatalov, J. Deng, X. Hu, J. Yang, A. Lunev, Y. Bilenko, M. Shur, and R. Gaska, *Efficiency droop in 245-247 nm AlGaN light-emitting diodes with continuous wave 2 mW output power*, Applied Physics Letters **96**, (2010).

[19] H. Hirayama, S. Fujikawa, N. Noguchi, J. Norimatsu, T. Takano, K. Tsubaki, and N. Kamata, *222-282 nm AlGaN and InAlGaN-based deep-UV LEDs fabricated on high-quality AlN on sapphire*, physica status solidi (a) **206**, 1176 (2009).

[20] A. A. Efremov, N. I. Bochkareva, R. I. Gorbunov, D. A. Lavrinovich, Y. T. Rebane, D. V. Tarkhin, and Y. G. Shreter, *Effect of the joule heating on the quantum efficiency and choice of thermal conditions for high-power blue InGaN/GaN LEDs*, Semiconductors **40**, 605 (2006).

[21] M.-H. Kim, M. F. Schubert, Q. Dai, J. K. Kim, E. F. Schubert, J. Piprek, and Y. Park, *Origin of efficiency droop in GaN-based light-emitting diodes*, Appl. Phys. Lett. **91**, 183507 (2007).

[22] A. Laubsch, M. Sabathil, W. Bergbauer, M. Strassburg, H. Lugauer, M. Peter, S. Lutgen, N. Linder, K. Streubel, J. Hader, J. V. Moloney, B. Pasenow, and S. W. Koch, *On the origin of IQE-?droop? in InGaN LEDs*, Phys. Status Solidi C **6**, S913 (2009).

[23] J. Hader, J. V. Moloney, B. Pasenow, S. W. Koch, M. Sabathil, N. Linder, and S. Lutgen, *On the importance of radiative and Auger losses in GaN-based quantum wells*, Applied Physics Letters **92**, (2008).

[24] K. Fujiwara, H. Jimi, and K. Kaneda, *Temperature-dependent droop of electroluminescence efficiency in blue (In,Ga)N quantum-well diodes*, physica status solidi (c) **6**, S814 (2009).

[25] X. Li, X. Ni, J. Lee, M. Wu, . Özgür, H. Morkoç, T. Paskova, G. Mulholland, and K. R. Evans, *Efficiency retention at high current injection levels in m-plane InGaN light emitting diodes*, Applied Physics Letters **95**, (2009).

[26] Y.-D. Lin, A. Chakraborty, S. Brinkley, H. C. Kuo, T. Melo, K. Fujito, J. S. Speck, S. P. DenBaars, and S. Nakamura, *Characterization of blue-green m-plane InGaN light emitting diodes*, Applied Physics Letters **94**, (2009).

[27] M. J. Davies, P. Dawson, S. Hammersley, T. Zhu, M. J. Kappers, C. J. Humphreys, and R. A. Oliver, *Comparative studies of efficiency droop in polar and non-polar InGaN quantum wells*, Applied Physics Letters **108**, (2016).

[28] J. Piprek, *Efficiency droop in nitride-based light-emitting diodes*, Phys. Status Solidi A **207**, 2217 (2010).

[29] Y. C. Shen, G. O. Mueller, S. Watanabe, N. F. Gardner, A. Munkholm, and M. R. Krames, *Auger recombination in InGaN measured by photoluminescence*, Appl. Phys. Lett. **91**, 141101 (2007).

[30] J. Iveland, L. Martinelli, J. Peretti, J. S. Speck, and C. Weisbuch, *Direct Measurement of Auger Electrons Emitted from a Semiconductor Light-Emitting Diode under Electrical Injection: Identification of the Dominant Mechanism for Efficiency Droop*, Phys. Rev. Lett. **110**, 177406 (2013).

[31] K. T. Delaney, P. Rinke, and C. G. Van de Walle, *Auger recombination rates in nitrides from first principles*, Appl. Phys. Lett. **94**, 191109 (2009).

[32] N. F. Gardner, G. O. Müller, Y. C. Shen, G. Chen, S. Watanabe, W. Götz, and M. R. Krames, *Blue-emitting InGaN?GaN double-heterostructure light-emitting diodes reaching maximum quantum efficiency above 200A?cm2*, Applied Physics Letters **91**, (2007).

[33] J. Hader, J. V. Moloney, and S. W. Koch, *Density-activated defect recombination as a possible explanation for the efficiency droop in GaN-based diodes*, Appl. Phys. Lett. **96**, 221106 (2010).

[34] I. A. Pope, P. M. Smowton, P. Blood, J. D. Thomson, M. J. Kappers, and C. J. Humphreys, *Carrier leakage in InGaN quantum well light-emitting diodes emitting at 480 nm*, Applied Physics Letters **82**, 2755 (2003).

[35] J. Xie, X. Ni, Q. Fan, R. Shimada, m. Özgür, and H. Morkoç, *On the efficiency droop in InGaN multiple quantum well blue light emitting diodes and its reduction with p-doped quantum well barriers*, Applied Physics Letters **93**, (2008).

[36] A. Hangleiter, C. Netzel, D. Fuhrmann, F. Hitzel, L. Hoffmann, H. Bremers, U. Rossow, G. Ade, and P. Hinze, *Anti-localization suppresses non-radiative recombination in GaInN/GaN quantum wells*, Phil. Mag. **87**, 2041 (2007).

[37] R. A. Oliver, S. E. Bennett, T. Zhu, D. J. Beesley, M. J. Kappers, D. W. Saxey, A. Cerezo, and C. J. Humphreys, *Microstructural origins of localization in InGaN quantum wells*, Journal of Physics D: Applied Physics **43**, 354003 (2010).

[38] T. J. Badcock, S. Hammersley, D. Watson-Parris, P. Dawson, M. J. Godfrey, M. J. Kappers, C. McAleese, R. A. Oliver, and C. J. Humphreys, *Carrier Density Dependent Localization and Consequences for Efficiency Droop in InGaN/GaN Quantum Well Structures*, Japanese Journal of Applied Physics **52**, 08JK10 (2013).

[39] K. T. Delaney, P. Rinke, and C. G. Van de Walle, *Erratum: "Auger recombination rates in nitrides from first principles" [Appl. Phys. Lett. 94, 191109 (2009)]*, Applied Physics Letters **108**, (2016).

[40] M. Brendel, A. Kruse, H. Jönen, L. Hoffmann, H. Bremers, U. Rossow, and A. Hangleiter, *Auger recombination in GaInN/GaN quantum well laser structures*, Appl. Phys. Lett. **99**, 031106 (2011).

[41] B. Galler, P. Drechsel, R. Monnard, P. Rode, P. Stauss, S. Froehlich, W. Bergbauer, M. Binder, M. Sabathil, B. Hahn, and J. Wagner, *Influence of indium content and temperature on Auger-like recombination in InGaN quantum wells grown on (111) silicon substrates*, Applied Physics Letters **101**, (2012).

[42] D. Schiavon, M. Binder, M. Peter, B. Galler, P. Drechsel, and F. Scholz, *Wavelength-dependent determination of the recombination rate coefficients in single-quantum-well GaInN/GaN light emitting diodes*, physica status solidi (b) **250**, 283 (2013).

[43] M. Zhang, P. Bhattacharya, J. Singh, and J. Hinckley, *Direct measurement of auger recombination in In0.1Ga0.9N/GaN quantum wells and its impact on the efficiency of In0.1Ga0.9N/GaN multiple quantum well light emitting diodes*, Appl. Phys. Lett. **95**, 201108 (2009).

[44] S. Chichibu, A. Uedono, B. A. Onuma, T. andHaskell, A. Chakraborty, T. Koyama, P. T. Fini, S. Keller, S. P. DenBaars, J. S. Speck, U. K. Mishra, S. Nakamura, S. Yamaguchi, S. Kamiyama, H. Amano, I. Akasaki, J. Han, and T. Sota, *Origin of defect-insensitive emission probability in In-containing (Al,In,Ga)N alloy semiconductors*, Nature Materials **5**, 810 (2006).

[45] S. F. Chichibu, T. Azuhata, M. Sugiyama, T. Kitamura, Y. Ishida, H. Okumura, H. Nakanishi, T. Sota, and T. Mukai, *Optical and structural studies in InGaN quantum well structure laser diodes*, Journal of Vacuum Science & Technology B **19**, 2177 (2001).

[46] K. Okamoto, A. Scherer, and Y. Kawakami, *Near-field scanning optical microscopic transient lens for carrier dynamics study in InGaN/aN*, Applied Physics Letters **87**, (2005).

[47] A. Kaneta, K. Okamoto, Y. Kawakami, S. Fujita, G. Marutsuki, Y. Narukawa, and T. Mukai, *Spatial and temporal luminescence dynamics in an InxGa1??N single quantum well probed by near-field optical microscopy*, Applied Physics Letters **81**, 4353 (2002).

[48] D.-S. Shin, D.-P. Han, J.-Y. Oh, and J.-I. Shim, *Study of droop phenomena in InGaN-based blue and green light-emitting diodes by temperature-dependent electroluminescence*, Appl. Phys. Lett. **100**, 153506 (2012).

[49] M. F. Schubert, S. Chhajed, J. K. Kim, E. F. Schubert, D. D. Koleske, M. H. Crawford, S. R. Lee, A. J. Fischer, G. Thaler, and M. A. Banas, *Effect of dislocation*

density on efficiency droop in GaInN/GaN light-emitting diodes, Appl. Phys. Lett. **91**, 231114 (2007).

[50] B.-J. Ahn, T.-S. Kim, Y. Dong, M.-T. Hong, J.-H. Song, J.-H. Song, H.-K. Yuh, S.-C. Choi, D.-K. Bae, and Y. Moon, *Experimental determination of current spill-over and its effect on the efficiency droop in InGaN/GaN blue-light-emitting-diodes*, Applied Physics Letters **100**, (2012).

[51] K. J. Vampola, M. Iza, S. Keller, S. P. DenBaars, and S. Nakamura, *Measurement of electron overflow in 450 nm InGaN light-emitting diode structures*, Applied Physics Letters **94**, (2009).

[52] J.-H. Song, H.-J. Kim, B.-J. Ahn, Y. Dong, S. Hong, J.-H. Song, Y. Moon, H.-K. Yuh, S.-C. Choi, and S. Shee, *Role of photovoltaic effects on characterizing emission properties of InGaN/GaN light emitting diodes*, Applied Physics Letters **95**, (2009).

[53] G. Popovici, H. Morkoc, and S. N. Mohammad, in Group III Nitride Semiconductor Compounds: Physics and Applications, edited by B. Gil (Oxford University Press, New York, 1998), Chap. 2: Deposition and properties of group III nitrides by molecular beam epitaxy, pp. 19-69.

[54] The band parameters were determined by Andreas Hangleiter from a fit to the measured absorption spectra of GaN and InN considering the excitonic gain.

[55] I. Vurgaftman, J. R. Meyer, and L. R. Ram-Mohan, *Band parameters for III-V compound semiconductors and their alloys*, J. Appl. Phys. **89**, 5815 (2001).

[56] A. A. Klochikhin, V. Y. Davydov, V. V. Emtsev, A. V. Sakharov, V. A. Kapitonov, B. A. Andreev, H. Lu, and W. J. Schaff, *Acceptor states in the photoluminescence spectra of n-InN*, Phys. Rev. B **71**, 195207 (2005).

[57] M. Goano, E. Bellotti, E. Ghillino, G. Ghione, and K. F. Brennan, *Band structure nonlocal pseudopotential calculation of the III-nitride wurtzite phase materials system. Part I. Binary compounds GaN, AlN, and InN*, J. Appl. Phys. **88**, 6467 (2000).

[58] M. Drechsler, D. Hofmann, B. Meyer, T. Detchprohm, H. Amano, and I. Akasaki, *Determination of the Conduction Band Electron Effective Mass in Hexagonal GaN*, Japanese Journal of Applied Physics **34**, L1178 (1995).

[59] J. S. Im, A. Moritz, F. Steuber, V. Härle, F. Scholz, and A. Hangleiter, *Radiative carrier lifetime, momentum matrix element, and hole effective mass in GaN*, Appl. Phys. Lett. **70**, 631 (1997).

[60] K. Kim, W. R. L. Lambrecht, B. Segall, and M. van Schilfgaarde, *Effective masses and valence-band splittings in GaN and AlN*, Phys. Rev. B **56**, 7363 (1997).

[61] M. Suzuki, and T. Uenoyama, *Strain effect on electronic and optical properties of GaN/AlGaN quantum-well lasers*, Journal of Applied Physics **80**, 6868 (1996).

[62] B. Meyer, D. Volm, A. Graber, H. Alt, T. Detchprohm, A. Amano, and I. Akasaki, *Shallow donors in GaN?The binding energy and the electron effective mass*, Solid State Communications **95**, 597 (1995).

[63] W. Walukiewicz, J. W. A. III, K. M. Yu, Z. Liliental-Weber, J. Wu, S. X. Li, R. E. Jones, and J. D. Denlinger, *Structure and electronic properties of InN and In-rich group III-nitride alloys*, Journal of Physics D: Applied Physics **39**, R83 (2006).

[64] J. Wu, W. Walukiewicz, K. M. Yu, J. W. Ager, E. E. Haller, H. Lu, and W. J. Schaff, *Small band gap bowing in $In_{1-x}Ga_xN$ alloys*, Appl. Phys. Lett. **80**, 4741 (2002).

[65] V. Davydov, A. Klochikhin, V. Emtsev, S. Ivanov, V. Vekshin, F. Bechstedt, J. FurthmÃ¼ller, H. Harima, A. Mudryi, A. Hashimoto, A. Yamamoto, J. Aderhold, J. Graul, and E. Haller, *Band Gap of InN and In-Rich InxGa1-xN alloys (0.36< x <1)*, physica status solidi (b) **230**, R4 (2002).

[66] T. Matsuoka, M. Nakao, H. Okamoto, H. Harima, and E. Kurimoto, *Experimental Consideration of Optical Band-Gap Energy of Wurtzite InN*, Japanese Journal of Applied Physics **42**, 2288 (2003).

[67] A. Bykhovski, B. Gelmont, and M. Shur, *The influence of the strain-induced electric field on the charge distribution in GaN-AlN-GaN structure*, J. Appl. Phys. **74**, 6734 (1993).

[68] A. Hangleiter, F. Hitzel, S. Lahmann, and U. Rossow, *Composition dependence of polarization fields in GaInN/GaN quantum wells*, Appl. Phys. Lett. **83**, 1169 (2003).

[69] T. Takeuchi, S. Sota, M. Katsuragawa, M. Komori, H. Takeuchi, H. Amano, and I. Akasaki, *Quantum-Confined Stark Effect due to Piezoelectric Fields in GaInN Strained Quantum Wells*, Japanese Journal of Applied Physics **36**, L382 (1997).

[70] A. Hangleiter, D. Fuhrmann, M. Grewe, F. Hitzel, G. Klewer, S. Lahmann, C. Netzel, N. Riedel, and U. Rossow, *Towards understanding the emission efficiency of nitride quantum wells*, Phys. Status Solidi A **201**, 2808 (2004).

[71] S. Watanabe, N. Yamada, M. Nagashima, Y. Ueki, C. Sasaki, Y. Yamada, T. Taguchi, K. Tadatomo, H. Okagawa, and H. Kudo, *Internal quantum efficiency of highly-efficient $In_xGa_{1-x}N$-based near-ultraviolet light-emitting diodes*, Appl. Phys. Lett. **83**, 4906 (2003).

[72] A. Kim, W. Götz, D. Steigerwald, J. Wierer, N. Gardner, J. Sun, S. Stockman, P. Martin, M. Krames, R. Kern, and F. Steranka, *Performance of High-Power AlInGaN Light Emitting Diodes*, Phys. Status Solidi A **188**, 15 (2001).

[73] M. Peter, A. Laubsch, W. Bergbauer, T. Meyer, M. Sabathil, J. Baur, and B. Hahn, *New developments in green LEDs*, Phys. Status Solidi A **206**, 1125 (2009).

[74] I. E. Titkov, S. Y. Karpov, A. Yadav, V. L. Zerova, M. Zulonas, B. Galler, M. Strassburg, I. Pietzonka, H. J. Lugauer, and E. U. Rafailov, *Temperature-Dependent Internal Quantum Efficiency of Blue High-Brightness Light-Emitting Diodes*, IEEE Journal of Quantum Electronics **50**, 911 (2014).

[75] M. R., M. Ochiai-Holcomb, G. E. Höfler, C. Carter-Coman, E. I. Chen, I.-H. Tan, P. Grillot, N. F. Gardner, H. C. Chui, J.-W. Huang, S. A. Stockman, F. A. Kish, M. G. Craford, T. S. Tan, C. P. Kocot, M. Hueschen, J. Posselt, B. Loh, G. Sasser, and D. Collins, *High-power truncated-inverted-pyramid (AlxGa1?x)0.5In0.5P/GaP light-emitting diodes exhibiting >50quantum efficiency*, Applied Physics Letters **75**, 2365 (1999).

[76] M. Yamada, T. Mitani, Y. Narukawa, S. Shioji, I. Niki, S. Sonobe, K. Deguchi, M. Sano, and T. Mukai, *InGaN-Based Near-Ultraviolet and Blue-Light-Emitting Diodes with High External Quantum Efficiency Using a Patterned Sapphire Substrate and a Mesh Electrode*, Japanese Journal of Applied Physics **41**, L1431 (2002).

[77] J. J. Wierer, M. R. Krames, J. E. Epler, N. F. Gardner, M. G. Craford, J. R. Wendt, J. A. Simmons, and M. M. Sigalas, *InGaN/GaN quantum-well heterostructure light-emitting diodes employing photonic crystal structures*, Applied Physics Letters **84**, 3885 (2004).

[78] I. Schnitzer, E. Yablonovitch, C. Caneau, T. J. Gmitter, and A. Scherer, *30light-emitting diodes*, Applied Physics Letters **63**, 2174 (1993).

[79] T. Fujii, Y. Gao, R. Sharma, E. L. Hu, S. P. DenBaars, and S. Nakamura, *Increase in the extraction efficiency of GaN-based light-emitting diodes via surface roughening*, Applied Physics Letters **84**, 855 (2004).

[80] D. Fuhrmann, U. Rossow, C. Netzel, H. Bremers, G. Ade, P. Hinze, and A. Hangleiter, *Optimizing the internal quantum efficiency of GaInN SQW structures for green light emitters*, physica status solidi (c) **3**, 1966 (2006).

[81] M. BORN, and E. WOLF, *Principles of Optics* (Pergamon, New York, 1980).

[82] D. A. B. Miller, D. S. Chemla, T. C. Damen, A. C. Gossard, W. Wiegmann, T. H. Wood, and C. A. Burrus, *Band-Edge Electroabsorption in Quantum Well Structures: The Quantum-Confined Stark Effect*, Phys. Rev. Lett. **53**, 2173 (1984).

[83] J. Im, H. Kollmer, J. Off, A. Sohmer, F. Scholz, and A. Hangleiter, *Reduction of oscillator strength due to piezoelectric fields in GaN/$Al_xGa_{1-x}N$ quantum wells*, Phys. Rev. B **57**, R9435 (1998).

[84] L.-H. Peng, C.-W. Chuang, and L.-H. Lou, *Piezoelectric effects in the optical properties of strained InGaN quantum wells*, Applied Physics Letters **74**, 795 (1999).

[85] J. Sheu, G. Chi, Y. Su, C. Liu, C. Chang, W. Hung, and M. Jou, *Luminescence of an InGaN/GaN multiple quantum well light-emitting diode*, Solid-State Electronics **44**, 1055 (2000).

[86] S. Sze, and K. K. Ng, in *Physics of Semiconductor Devices* (John Wiley & Sons, Inc., Hoboken, NJ, USA, 2006), pp. 77–133.

[87] H. Jönen, H. Bremers, U. Rossow, T. Langer, A. Kruse, L. Hoffmann, J. Thalmair, J. Zweck, S. Schwaiger, F. Scholz, and A. Hangleiter, *Analysis of indium incorporation in non- and semipolar GaInN QW structures: comparing x-ray diffraction and optical properties*, Semiconductor Science and Technology **27**, 024013 (2012).

[88] F. Zhang, M. Ikeda, K. Zhou, Z. S. Liu, J. P. Liu, S. M. Zhang, and H. Yang, *Current density dependence of transition energy in blue InGaN/GaN MQW LEDs*, physica status solidi (c) **13**, 256 (2016).

[89] Y.-L. Li, Y.-R. Huang, and Y.-H. Lai, *Efficiency droop behaviors of InGaN/GaN multiple-quantum-well light-emitting diodes with varying quantum well thickness*, Appl. Phys. Lett. **91**, 181113 (2007).

[90] A. David, and M. J. Grundmann, *Droop in InGaN light-emitting diodes: A differential carrier lifetime analysis*, Applied Physics Letters **96**, (2010).

[91] Q. Dai, Q. Shan, J. Cho, E. F. Schubert, M. H. Crawford, D. D. Koleske, M.-H. Kim, and Y. Park, *On the symmetry of efficiency-versus-carrier-concentration curves in*

GaInN/GaN light-emitting diodes and relation to droop-causing mechanisms, Applied Physics Letters **98**, (2011).

[92] A. Laubsch, M. Sabathil, J. Baur, M. Peter, and B. Hahn, *High-Power and High-Efficiency InGaN-Based Light Emitters*, IEEE Trans. Electron Devices **57**, 79 (2010).

[93] M. Meneghini, N. Trivellin, G. Meneghesso, E. Zanoni, U. Zehnder, and B. Hahn, *A combined electro-optical method for the determination of the recombination parameters in InGaN-based light-emitting diodes*, J. Appl. Phys. **106**, 114508 (2009).

[94] A. Hangleiter, T. Langer, M. Gerhard, D. Kalincev, A. Kruse, H. Bremers, U. Rossow, and M. Koch, Efficiency droop in nitride LEDs revisited: impact of excitonic recombination processes, 2015.

[95] T. Langer, A. Chernikov, D. Kalincev, M. Gerhard, H. Bremers, U. Rossow, M. Koch, and A. Hangleiter, *Room temperature excitonic recombination in GaInN/GaN quantum wells*, Applied Physics Letters **103**, (2013).

[96] A. Hangleiter, Z. Jin, M. Gerhard, D. Kalincev, T. Langer, H. Bremers, U. Rossow, M. Koch, M. Bonn, and D. Turchinovich, *Efficient formation of excitons in a dense electron-hole plasma at room temperature*, Phys. Rev. B **92**, 241305 (2015).

[97] S. Sze, and K. K. Ng, in *Physics of Semiconductor Devices* (John Wiley & Sons, Inc., Department of Electronics Engineering, National Chiao Tung University, Hsinchu, Taiwan, 2006), pp. 5–75.

[98] P. Basu, *Theory of Optical Processes in Semiconductors: Bulk and Microstructures* (Clarendon Press, Oxford, 1997).

[99] A. Rubio, J. L. Corkill, M. L. Cohen, E. L. Shirley, and S. G. Louie, *Quasiparticle band structure of AlN and GaN*, Phys. Rev. B **48**, 11810 (1993).

[100] M. Suzuki, T. Uenoyama, and A. Yanase, *First-principles calculations of effective-mass parameters of AlN and GaN*, Phys. Rev. B **52**, 8132 (1995).

[101] Y. C. Yeo, T. C. Chong, and M. F. Li, *Electronic band structures and effective-mass parameters of wurtzite GaN and InN*, J. Appl. Phys. **83**, 1429 (1998).

[102] A. Hangleiter, S. Heppel, J. Off, B. Kuhn, F. Scholz, S. Bader, B. Hahn, and V. Härle, *Analysis of the threshold current in nitride-based lasers*, J. Cryst. Growth **230**, 522 (2001).

[103] A. Hangleiter, J. Im, J. Off, and F. Scholz, *Optical Properties of Nitride Quantum Wells: How to Separate Fluctuations and Polarization Field Effects*, Phys. Status Solidi B **216**, 427 (1999).

[104] W. Shockley, and W. T. Read, *Statistics of the Recombinations of Holes and Electrons*, Phys. Rev. **87**, 835 (1952).

[105] R. Hall, *Electron-Hole Recombination in Germanium*, Phys. Rev. **87**, 387 (1952).

[106] A. Getty, E. Matioli, M. Iza, C. Weisbuch, and J. S. Speck, *Electroluminescent measurement of the internal quantum efficiency of light emitting diodes*, Applied Physics Letters **94**, (2009).

[107] E. Matioli, and C. Weisbuch, *Direct measurement of internal quantum efficiency in light emitting diodes under electrical injection*, Journal of Applied Physics **109**, (2011).

Acknowledgement

All the work would not have been achieved without the help and support of many people, whom I would gratefully acknowledge here.

- First of all I would like to thank my supervisor Prof. Dr. Andreas Hangleiter. Without his patient guidance and support, I would never been able to complete this work. He also always taught me how to do scientific research in a correct way, which will benefit me for the whole life.
- Prof. Dr. Stefan Kück for the adoption of the second report.
- I also want to give further and great thanks to all my current and former colleagues in our institute: Dr.Uwe Rossow offered me lots of information about LED samples and solutions for experimental set up. Dr. Torsten Langer have numerous and helpful discussions with me, which make me improve quickly. Dr. Jayanta Kumar Mishra was always very friendly and give me many useful suggestions. Fedor Alexej Ketzer give me many assistance on the measurements. Andreas Kruse help me a lot on adapt the new life in Germany at the beginning. Dr. Heiko Bremers, Dr. Lars Hoffmann, Dr. Andreas Kraus, Dr. Holger Jönen, Moritz Brendel, Dr. Ernst Ronald Buß, Peter Clodius, Manuela Klisch, Christopher Hein, Philipp Horenburg, Markus Göthlich, Dennis Mauch.
- Ingeborg Westphal, Diana Deuse and the workshop team headed by Frank Werner for uncomplicated technical support and Dagmar Schumacher for assistance in administrative matters.
- For the pleasant working atmosphere, I would like to thank all the staff in Institut für Angewandte Physik, also among those whom I have not yet mentioned.
- I also would like to specially thank my family for their unconditional love and encouragement during every stage of my life.